Protist, Vol. 168, 586–611, xx 2017
http://www.elsevier.de/protis
Published online date 9 September 2017

Protist

ORIGINAL PAPER

Ultrastructure and Phylogeny of *Kirithra asteri* gen. et sp. nov. (Ceratoperidiniaceae, Dinophyceae) — a Free-Living, Thin-Walled Marine Photosynthetic Dinoflagellate from Argentina

Pernille Vængebjerg Boutrup[a], Øjvind Moestrup[a], Urban Tillmann[b], and Niels Daugbjerg[a,1]

[a]Marine Biological Section, University of Copenhagen, Universitetsparken 4, 2100 Copenhagen Ø, Denmark
[b]Alfred-Wegener-Institut, Helmholtz-Zentrum für Polar-und Meeresforschung, Am Handelshafen 12, Bremerhaven 27570, Germany

Submitted May 16, 2017; received in revised form August 22, 2017; Accepted August 26, 2017
Monitoring Editor: Mona Hoppenrath

A gymnodinioid photosynthetic dinoflagellate was isolated from Argentina and examined by light and electron microscopy and analysis of nuclear-encoded LSU rDNA. *Kirithra asteri* gen. et sp. nov. was proposed as morphology and molecular phylogeny separated this dinoflagellate from others within the family Ceratoperidiniaceae. Cells were surrounded by a hyaline amphiesma comprising polygonal vesicles. Each vesicle contained a honeycomb and a trilaminar structure. An anterior sulcal extension ending in a complete circle formed the apical structure complex (ASC), which characterizes Ceratoperidiniaceae. The ASC comprised three rows of vesicles. The nucleus was located in the hypocone, and several large, irregularly shaped vesicles were present in the epi- and hypocone. Chloroplasts were surrounded by three membranes, and grana-like arrangements of thylakoids were observed in one strain used for ultrastructural study. The cell centre contained 1-3 multiple-stalked pyrenoids and membrane-bound vesicles containing tile-like structures surrounded each pyrenoid. Two pusules with collecting chambers and associated vesicles branched off each of the flagellar canals. The flagellar apparatus featured a ventral connective between the amphiesma and the R1 root, and almost opposite basal bodies, rarely seen in dinoflagellates. This was the first ultrastructural study of a species within Ceratoperidiniaceae.

Keywords: Apical structure complex; autotrophic dinoflagellates; Ceratoperidiniaceae; molecular phylogeny; ultrastructure.

[1]Corresponding author;
e-mail n.daugbjerg@bio.ku.dk (N. Daugbjerg).

http://dx.doi.org/10.1016/j.protis.2017.08.001

Introduction

Thirty-seven years ago Loeblich III (1980) created the new monotypic dinoflagellate family Ceratoperidiniaceae, to include the genus *Ceratoperidinium* Loeblich III *emend*. Réñe & de Salas, a genus originally described (albeit invalidly, Latin diagnosis missing) by Margalef (1969) in an article on phytoplankton from the Mediterranean. Loeblich validated the generic name and gave the single species a new name, *C. margalefii* Loeblich III, to replace Margalef's invalid name *C. yeye* Margalef. A few years later, a second species was described from the Lebanese coast, *C. mediterraneum* Abboud-Abi Saab (1989), but it was subsequently considered a synonym of *C. margalefii* by Gómez et al. (2004), this species being morphologically very variable. The third taxon included in the family was originally described as *Gymnodinium fusus* Schütt (1895; synonym: *Gyrodinium falcatum* Kofoid & Swezy, see Elbrächter 1979). It was transferred to *Ceratoperidinium* as *C. falcatum* (Kofoid & Swezy) Réñe & de Salas. It is a very widely distributed species which varies considerably in morphology, and Konovalova (2003) reported that a species named *Pseliodinium vaubanii* Sournia (Sournia 1972), is in fact a stage in the life cycle of this species. There is a high level of plasticity in the morphology of the described species of the family, making species identification and circumscription difficult. The phylogenetic analysis published, however, show that material identified as *C. falcatum* locates in different positions in the phylogenetic trees, indicating that additional species may exist. The phylogenetic trees also include material identified as *Gymnodinium* sp. 1, *Cochlodinium* cf. *helix* and *Cochlodinium* cf. *convolutum* (Reñé et al. 2013).

The family thus comprises only two species described in some detail, although the ultrastructure of both species remains unknown, *C. margalefii* from the Mediterranean and *Gymnodinium fusus*, which is distributed worldwide. During a cruise in Argentinian waters, a thin-walled dinoflagellate was encountered and isolated into culture which, although morphologically very different from the two known species, was found to represent a new genus of the family. The culture was examined by light and electron microscopy and the phylogeny investigated based on nuclear-encoded LSU rDNA gene sequences. It is described here as *Kirithra asteri* gen. et sp. nov.

Results

Taxonomic Descriptions

Kirithra Boutrup, Tillmann, Daugbjerg & Moestrup gen. nov.

DIAGNOSIS: Cells motile and free-living. Thin-walled, but the amphiesmal vesicles contain both a honeycomb layer and a trilaminar layer. Apical structure complex forms a complete circle, consisting of three parallel series of vesicles, the central one possessing knobs. Flagellar basal bodies of almost opposite polarity. Ventral connective associated with R1 flagellar root. Chloroplasts surrounded by three membranes, with centrally placed pyrenoids. Trichocysts present.

TYPE SPECIES: *Kirithra asteri* Boutrup, Tillmann, Daugbjerg & Moestrup sp. nov.

ETYMOLOGY: Greek κηρήθρα, "honeycomb", from the elaborate honeycomb layer present in the amphiesmal vesicles.

Kirithra asteri Boutrup, Tillmann, Daugbjerg & Moestrup sp. nov.

DIAGNOSIS: Cells ovoid with conical epicone and slightly larger hemispherical hypocone. Somewhat flattened on ventral side. Length interval 26–41 μm (average 32.1 ± 3.3 μm); width interval 18–30 μm (average 23.8 ± 3.0) (n = 62). Cingulum median, descending and displaced 1-2 cingulum widths. Sulcus widens posteriorly, and almost reaches the antapex. Commencement of cingulum and sulcus in invaginations of the amphiesma covered by ventral ridge. Amphiesma of small polygonal vesicles, with pores in the junctions only. Yellowish-brown chloroplasts form a reticulated network radiating from 1-3 centrally placed pyrenoids. Chloroplasts sometimes contain grana-like structures. Pyrenoids multi-stalked, surrounded by membrane-bound vesicles, which contain tile-like structures. Pyrenoids not penetrated by thylakoids, but invaginated by finger-like extensions from the surrounding vesicles. Eyespot and peduncle absent. Nucleus spherical, located in the hypocone, typical nuclear pores separate or in small groups. Two collecting chamber pusules with vesicles connects with each of the flagellar canals. Asexual reproduction by fission in the motile stage. Nuclear-encoded LSU rDNA gene sequence = GenBank accession number MF666674.

HOLOTYPE: An epon-embedded sample of the clonal culture established from material collected

9 September 2015, has been deposited at the Botanical Museum, University of Copenhagen (C), accession no. C-A-92079.

TYPE LOCALITY: Argentinian ocean shelf, South Atlantic Ocean (41°10′48″S, 57°51′36″W)

ETYMOLOGY: Greek αστείρι, "star", refers to the refractive nature of the vesicles surrounding the pyrenoid when viewed in8 the light microscope.

Light and Epifluorescence Microscopy

Cells of *Kirithra asteri* (Fig. 1A-I) were ovoid in shape, widest posteriorly, with a hemispherical hypocone, and a conical epicone rounded apically (Fig. 1A-H). The cingulum was deeply engraved and extended more or less vertically from the transverse flagellar canal on the ventral side, made a 90-degree turn and descended slightly in a leftwards spiral, the ends displaced approximately 1-2 cingular widths (Fig. 1A-B). The exits of the longitudinal and transverse flagella were covered by the ventral ridge upon which was a delicate furrow (Fig. 1A-B). The sulcus widened below the ventral ridge, and a thin sulcal extension could be seen invading the epicone for a short distance above the proximal part of the cingulum (Fig. 1A). The ventral side of the cell was somewhat flattened (Fig. 1E). Chloroplasts forming a reticulated network were primarily located close to the cell surface (Fig. 1A-D) but also radiated from the centrally placed pyrenoids (Fig. 1F). The spherical pyrenoids (1-3 in each cell) were placed on level with the cingulum, or sometimes shifted a short distance into the epicone (not shown). Pyrenoids were surrounded by material that refracted the light (Fig. 1F-G). The nucleus was large, spherical and placed centrally in the hypocone (Fig. 1F-H, M). The cell apex was delimited by a furrow and was rounded and more protuberant than the rest of the epicone (Fig. 1E-H). Cells exposed to stress under the microscope sometimes exhibited a pointed apex (Fig. 1I) and the hyaline amphiesma often moved away from the cell (Figs 1H-I, K-L). The hyaline polygonal amphiesmal vesicles could sometimes be seen where the amphiesma had lost contact with the cytoplasm (Fig. 1J). The amphiesma remained intact during cell division, which began in the hypocone (Fig. 1K-L, N-P), the nucleus becoming kidney-shaped with one end in each of the two hypocones (Fig. 1K). Cells were motile and did not discard the amphiesma during cell division.

In epifluorescence microscopy with green light excitation chloroplasts were visualized to form a reticulated network (Fig. 1M-P). A vegetative cell with chloroplasts stained with DAPI revealed chloroplast DNA as blue dots (Fig. 1M). Three different stages of cell division are illustrated in Figs 1N-P. In the first stage (Fig. 1N) the nucleus has moved to the epicone. In the second stage (Fig. 1O) the nucleus has moved back to the hypocone and is in the process of karyokinesis. The third stage (Fig. 1P) is similar to the cell in Figure 1L. Each daughter cell has its own nucleus in what will become the hypocone of the new cells.

Scanning Electron Microscopy

Details of cell morphology are illustrated in Figure 2A-F. The ventral side of the cell displayed the transverse flagellum emerging vertically from behind the ventral ridge. It made a 90° leftward turn and extended in the cingulum in a slightly downwards spiral around the cell. The cingulum terminated in a downwards slope, at the exit point of the longitudinal flagellum (Fig. 2A). The longitudinal flagellum often curled up into the broad sulcus (Fig. 2A, C). The ventral ridge covered the exit points of the two flagella and consisted of a central ridge lined on each side by a delicate furrow (Fig. 2A, C, seen as one furrow in Fig. 1A-B). The sulcal extension on the epicone continued in an anterior direction on the epicone to reach the apical structure complex (ASC) (Fig. 2A, F). At higher magnification, the sulcal extension was seen to consist of two elongate amphiesmal vesicles, the topmost of which connected with the amphiesmal vesicle of the ASC (Fig. 2F). Just above the start of the cingulum, next to the lowermost part of the sulcal extension, a distinct ventral pore could be seen (Fig. 2A, F). The dorsal side of the cell is shown in Figure 2B. The cell surface was covered by small polygonal amphiesmal vesicles, arranged in 7-10 latitudinal rows on each side of the cingulum. Most vesicles were 5- or 6-sided. The cingulum was 5 to 7 amphiesmal vesicles high (Figs 2B, 4A), the posterior row of vesicles notably smaller. The hypocone formed a smooth hemisphere, only interrupted by the sulcus, which continued almost to the antapex. The delineation of the broad sulcus was not clearly defined (Fig. 2A, C). The apex of the cell was encircled by the ASC (Fig. 2D, F) and appeared to consist of three rows of vesicles: a single, narrow, elongated amphiesmal vesicle with a central row of knobs releasing mucilaginous material (Fig. 2D-E), lined on each side by a row of somewhat larger vesicles (Fig. 13). The amphiesmal vesicles within the ASC were arranged with one central vesicle (some-

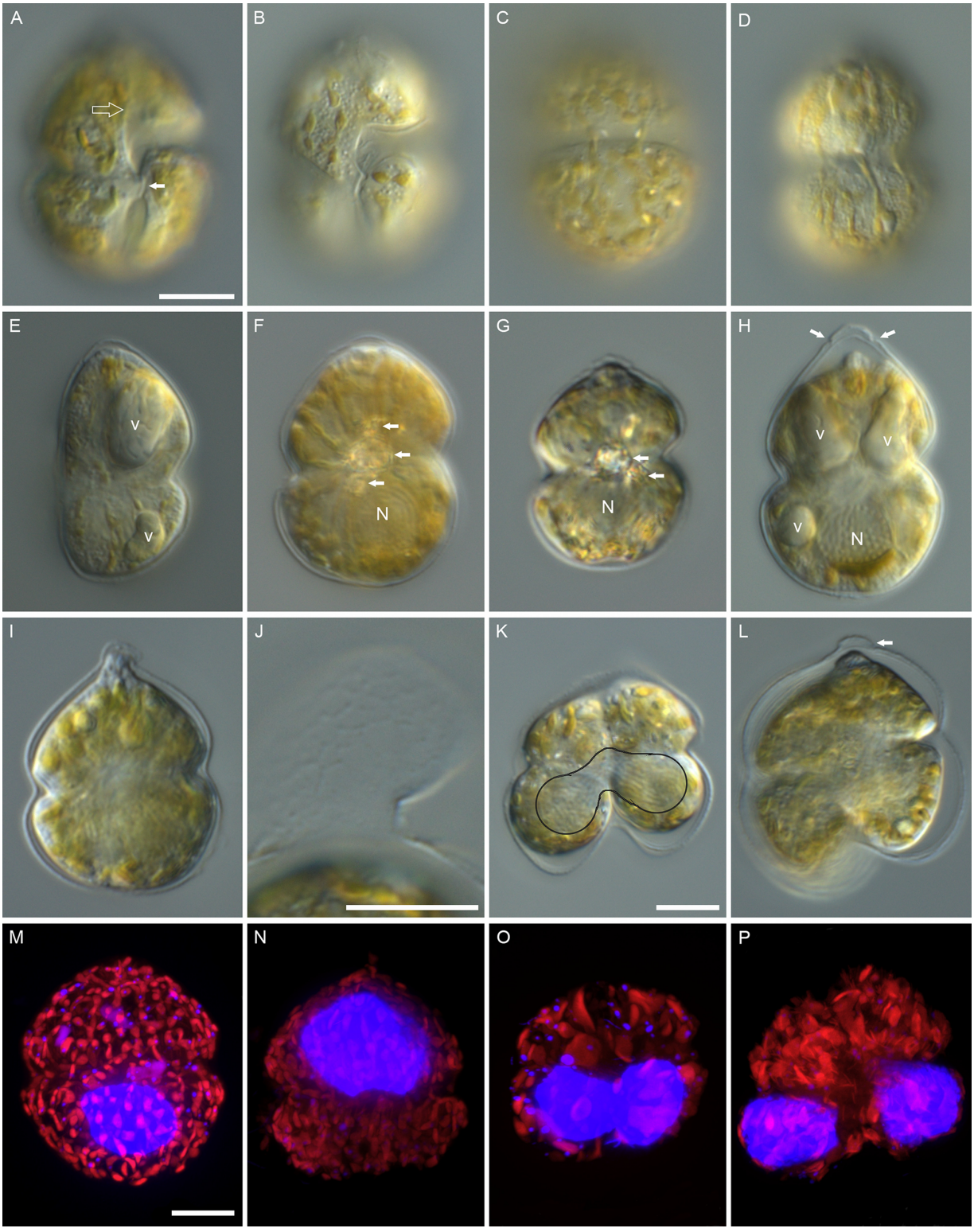

Figure 1. Light microscopy (A-L) and epifluorescence (M-P) of *Kirithra asteri* gen. et sp. nov. Scale bars = 10 μm. **A**) Ventral view of ovoid cell with slightly displaced cingulum, sulcus and ventral ridge with a delicate furrow (small arrow). A short sulcal extension is visible (open arrow). **B**) Ventral view of cell, showing cingulum edges, ventral ridge with delicate furrow and distal end of cingulum making a downwards turn

times two, not shown) encircled by approximately eight vesicles (Fig. 2D).

Dividing cells are shown in more detail in Figure 3A-B. The ventral side of a dividing cell displayed the longitudinal division furrow, in which the left daughter cell (right in the figure) retained the apical structure and the transverse flagellum, whereas the daughter cell to the left in the figure shifted downwards and retained the longitudinal flagellum (Fig. 3A). The dorsal side of a dividing cell at a slightly earlier state was very broad (Fig. 3B), while the hypocone was in the process of division, the cingulum was still intact (Fig. 3B).

Transmission Electron Microscopy

General ultrastructure: Although in many ways *Kirithra asteri* displayed a typical dinoflagellate ultrastructure, it also possessed some uncommon features. The dinokaryon contained regularly arranged condensed chromosomes and was positioned centrally in the hypocone (Fig. 4B-C). The nuclear envelope was penetrated by typical nuclear pores, which were placed individually (Fig. 7C) or in small groups (Fig. 7D). Mucocysts were absent, but trichocysts were distributed more or less evenly throughout the cell (Figs 4A, C, 6G). Several Golgi bodies surrounded the pyrenoid (Fig. 4B). Large irregularly shaped and seemingly empty vesicles were present in both the epi- and hypocone (Fig. 4A-B). An unusual type of vesicle with electron-dense multi-layered centre (Fig. 4F-G) occurred in large numbers in the cytosol, the highest numbers near the amphiesma (Figs 4A-C, 5C). The amphiesma formed two invaginations behind (below) the ventral ridge, creating cavities into which the flagella emerged; the transverse and longitudinal amphiesmal invagination (TAI and LAI, Figs 4B, D-E, 8E, 9A-D, J-K). The invagination of the transverse flagellum was supported by rows (sheets) of microtubules (Fig. 4D-E). The longitudinal flagellum contained cross-hatched packing material and a muscle-like striated fibre (Figs 4H, 8E).

Amphiesma: A distinct trilaminar layer (dark-light-dark) was present within the amphiesmal vesicles. It was observed as a separate unit within each amphiesmal vesicle (Fig. 5A), or the units had fused to form an unbroken layer that enclosed the whole cell (Fig. 5B). In the latter case, all junctions between the outer- and inner amphiesmal vesicle membranes were broken, and the inner amphiesmal vesicle membranes had fused to form an unbroken membrane surrounding the cytoplasm (Fig. 5B). The amphiesmal vesicles did not contain plates, but an elaborate honeycomb layer was present between the outer amphiesmal vesicle membrane and the trilaminar layer (Fig. 5A-B, D-E). The honeycomb pattern was most obvious when sectioned tangentially (Fig. 5F-G), and at other angles appeared fibrillar (Fig. 5A-B) or as thin filaments (Fig. 5D). Each unit of the honeycomb was approximately 40 nm in diameter (Fig. 5G). Amphiesmal pores were only present in the junctions between the vesicles (Fig. 5F-G).

Apical structure complex: In longitudinal sections of the cell, the apical structure complex (ASC) was visible on each side of the cell apex (Fig. 5C), comprising a narrow vesicle, lined on each side by a larger vesicle. These latter vesicles resembled normal amphiesmal vesicles, but were smaller. The narrow central vesicle lacked the trilaminar layer, but was subtended on the cytoplasmic side by a microtubule, sometimes with indication of a second microtubule (Fig. 5D), and carried the knobs releasing mucilaginous material (Fig. 5E).

towards the longitudinal flagellum. Both flagella present, although barely visible. **C**) Dorsal view of cell with a broad cingulum and chloroplasts in reticulated network. **D**) Dorsal side of cell in a slightly deeper focal plane showing chloroplasts arrangement. **E**) Left side of a cell showing ventral flattening, and two large irregularly shaped vesicles (v). **F**) Deep focal plane displaying nucleus (N), three pyrenoids, one large central and two smaller (arrows), from which bands of chloroplasts radiate into the epicone. **G**) Deep focal plane of smaller cell containing two pyrenoids (arrows), and nucleus (N). **H**) Deep focal level of slightly stressed cell in which the cytoplasm has retracted from the amphiesma in the top-most part of the epicone, revealing the apical structure complex (arrows). Nucleus (N) and three somewhat irregularly shaped vesicles (v) also visible. **I**) Deep focal plane of cell showing apex sometimes pointed. **J**) Hyaline amphiesma detached from cell surface displaying small polygonal amphiesmal vesicles. **K**) Dividing cell displaying nucleus in karyokinesis. Edges of kidney-shaped nucleus outlined in black. Intact hyaline amphiesma around hypocones. **L**) Dividing cell with intact amphiesma somewhat detached from cytoplasm, showing the apical structure complex (arrow). **M**) Epifluorescence of vegetative cell exhibiting large spherical nucleus (blue) and numerous chloroplasts (red) most of which have associated small blue dots representing chloroplast DNA. **N**) Early stage cell division showing double-sized nucleus in the epicone. **O**) Dividing cell during karyokinesis. Chloroplast DNA clearly visible (blue dots). **P**) Late stage of cell division after karyokinesis; cytokinesis is not complete.

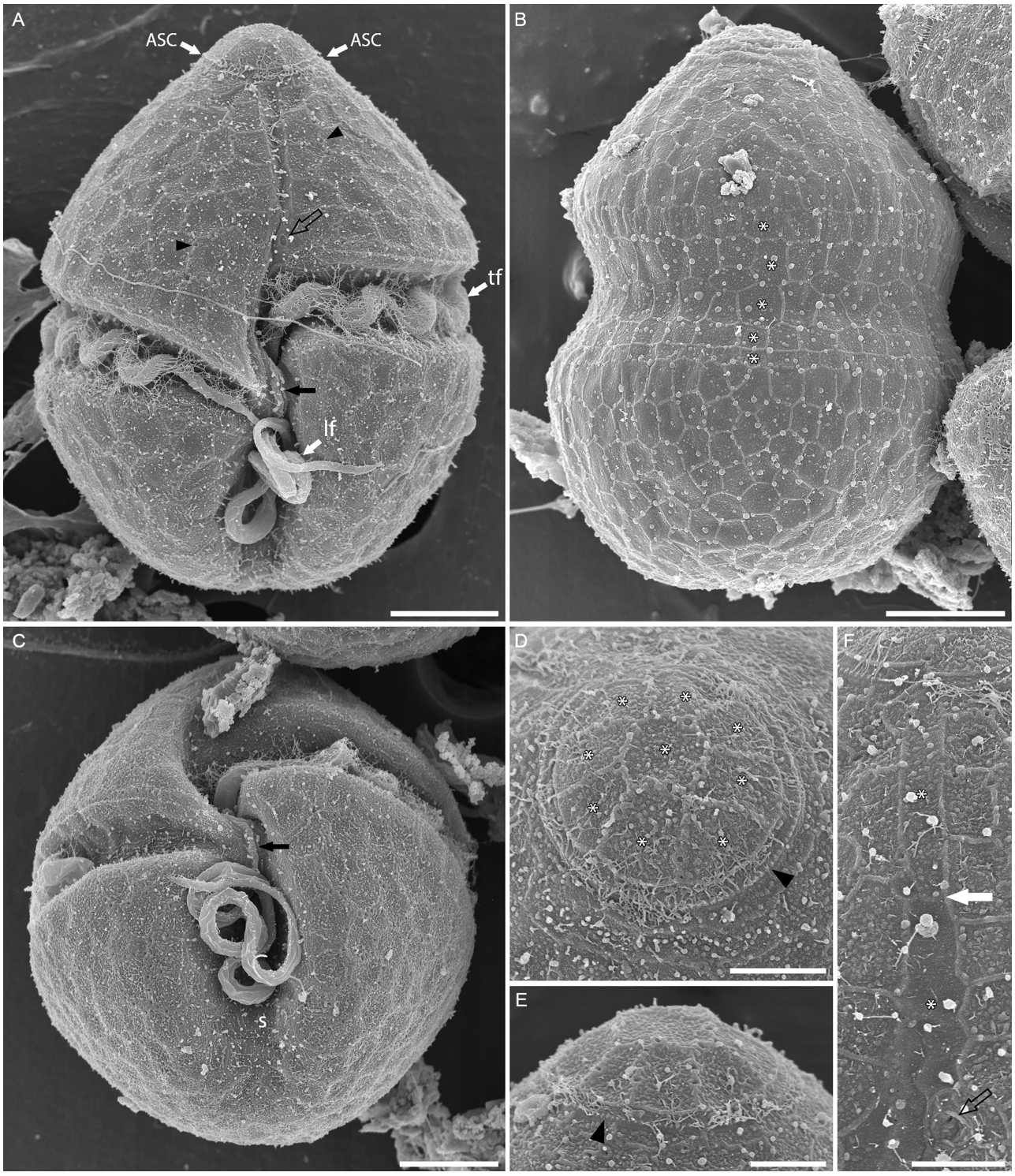

Figure 2. Scanning electron microscopy of *Kirithra asteri* gen et sp. nov. Scale bars: A-C = 5 μm, D-F = 2 μm. **A**) Ventral view of cell with smooth surface covered in polygonal amphiesmal vesicles. Transverse flagellum (tf) and longitudinal flagellum (lf). Numerous pores penetrate junctions of amphiesmal vesicles (two indicated with arrowheads). Ventral ridge with delicate furrows on each side (arrow). Sulcal extension runs from topmost part of cingulum to the apical structure. The apical structure complex (ASC) is circular. A large conspicuous pore is present in the lowermost part of the sulcal extension (open arrow). **B**) Dorsal view of cell with broad

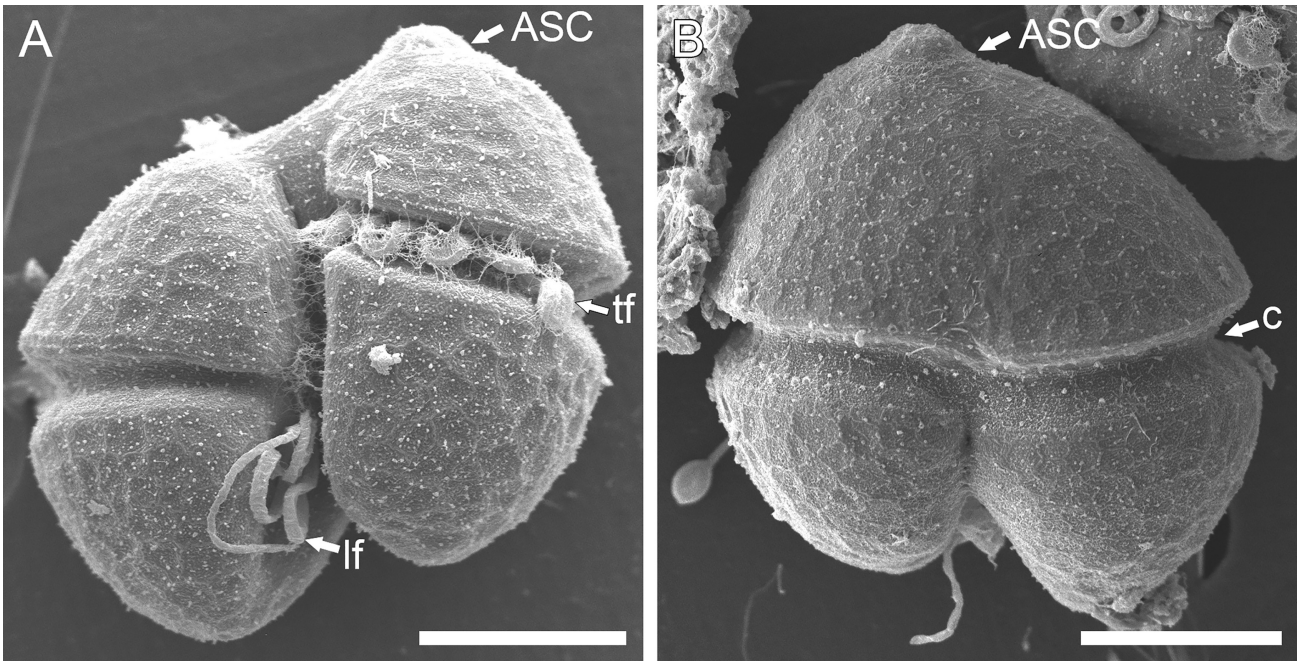

Figure 3. Scanning electron microscopy of dividing cells of *Kirithra asteri* gen. et sp. nov. Scale bars = 10 μm. **A**) Ventral view of dividing cell. Cells are still connected in the epicones and the amphiesma is intact. The apical structure complex (ASC) and the transverse flagellum (tf) are located on the right daughter cell, the longitudinal flagellum (lf) on the left daughter cell. **B**) Dorsal view of dividing cell displaying longitudinal division in hypocone and intact cingulum (c) and amphiesma.

Pyrenoids: The pyrenoids were multiple-stalked and located centrally in the cell, connected to radiating chloroplasts (Figs 4B, 6B). Three membranes lined each pyrenoid (Fig. 6F). The pyrenoid matrix was uniformly granular and penetrated by tube-like invaginations of the surrounding membrane-bound pyrenoid vesicles (Fig. 6A-B), usually several tubes in each invagination (Fig. 6C, D). At higher magnification the three membranes lining the pyrenoid were seen to be tightly appressed the inner membrane of a vesicle, to give the impression of four membranes (Fig. 6C, F). The vesicles lining the pyrenoid contained tile-like elements but such structures were not observed within the penetrations into the pyrenoid. Similar tile-containing vesicles also occurred elsewhere in the cell (not shown), although in the highest number around the pyrenoids (Figs 4B, 6A-B).

Chloroplasts: The chloroplasts formed a reticulated network, each part often were lens-shaped or elongated, and radiating from the centrally placed pyrenoids or located peripherally (Fig. 4A-C). They displayed a large area devoid of thylakoids, but containing chloroplast DNA (Fig. 6E, H). The thylakoids were generally stacked two or three together (Fig. 6E). The chloroplasts fixed for sectioning according to fixation schedule 2 all showed extensive grana formation of the thylakoids (Fig. 6G-H), whereas none of the chloroplasts from fixation schedule 1 showed any indication of grana formation.

Pusules: The two pusules were placed centrally in the cell's ventral area, each composed of pusule vesicles and a short broad collecting chamber (Figs 4A-B, 7A). The chambers converted into flagellar canals close to the striated collars with no vis-

cingulum consisting of five amphiesmal vesicles (asterisks). **C**) Antapical view of cell showing smoothly rounded hypocone with broad sulcus (s) continuing almost to the antapex. Ventral ridge indicated by arrow. **D-E**) Circular apical structure complex (ASC) from two different cells seen at higher magnification (arrowheads). Within the circular ASC is a central amphiesmal vesicle encircled by approximately eight amphiesmal vesicles (asterisks). **F**) Higher magnification of sulcal extension consisting of two elongated amphiesmal vesicles (asterisks). The junction between the vesicles is barely visible (white arrow). The uppermost part of the extension connects to the amphiesmal vesicle of the ASC. The large pore shown in Figure 2A is also visible (open arrow).

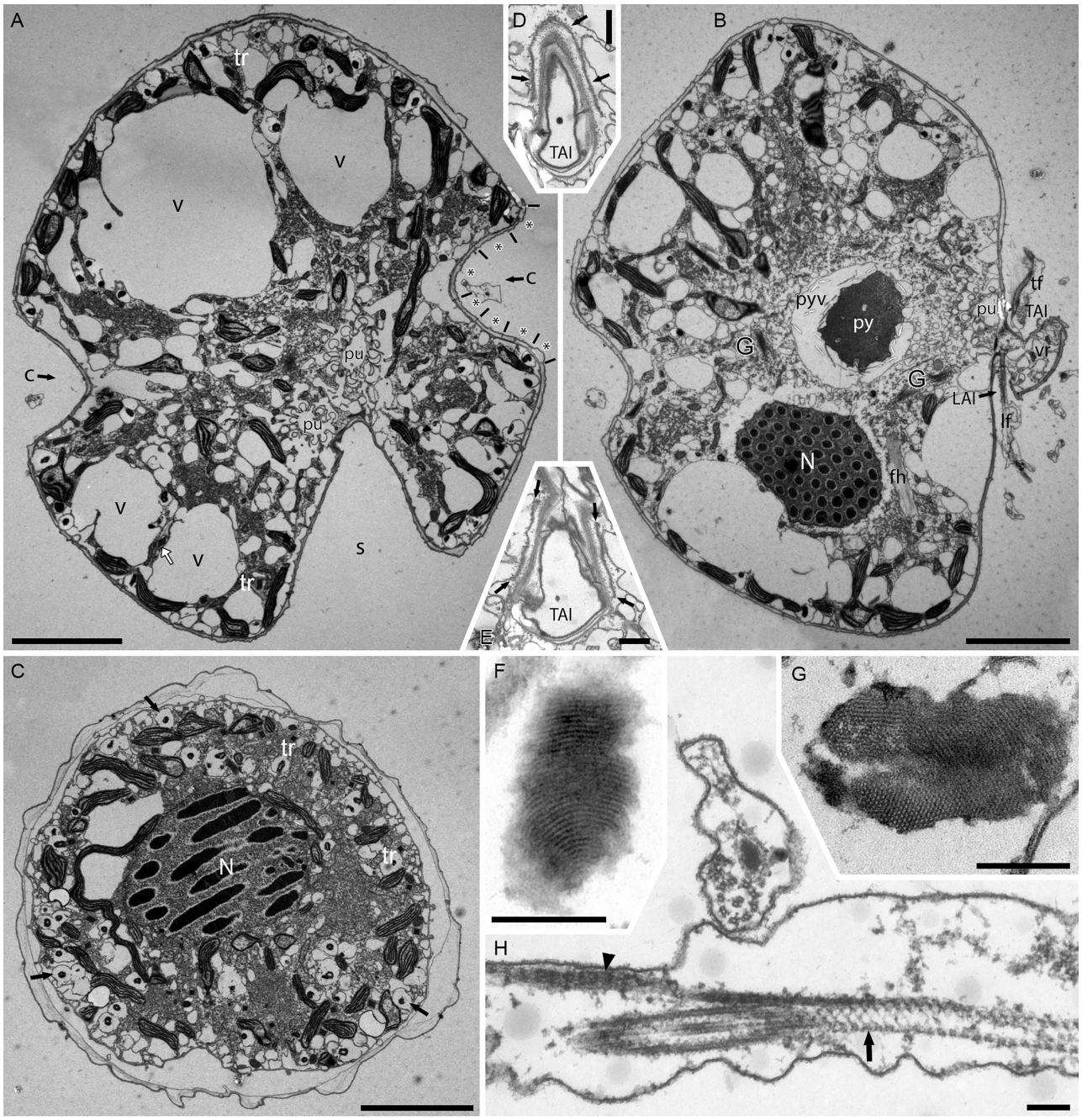

Figure 4. Transmission electron microscopy (TEM) of *Kirithra asteri* gen. et sp. nov. General ultrastructure, vesicle content and longitudinal flagellum. All fixed according to schedule 1. Scale bars: A-C = 5 μm, D-E = 500 nm, F-H = 200 nm. **A**) Longitudinal section in a frontal plane showing deep cingulum (c) and sulcus (s). The 7 amphiesma vesicles lining the cingulum in this specimen are marked by asterisks. Two pusules are visible in the sulcal area (pu). Chloroplasts line the cell periphery or radiate inwards. Large irregularly shaped vesicles (v) are present in epi- and hypocone. Trichocysts (tr) are distributed more or less evenly. **B**) Longitudinal section in sagittal plane, ventral side on the right, dorsal side on the left. A large centrally placed pyrenoid (py) is surrounded by membrane-bound vesicles containing tile-like inclusions (pyv). These vesicles are surrounded by Golgi bodies (G). The nucleus (N) is located centrally in the hypocone. Oppositely oriented flagella visible; transverse flagellum (tf) and longitudinal flagellum (lf). A ventral ridge (vr) covers the transverse and longitudinal amphiesmal invaginations (TAI and LAI, respectively). A pusule connects to the transverse flagellar pore (pu),

ible transition, other than pusule vesicles being replaced by collared pits near the opening (Figs 7A, 9A, K). Collecting chambers were approximately 2.5 to 2.8 μm long and enclosed by a single membrane. Closely packed pusule vesicles lined the collecting chambers and opened into the chambers by narrow apertures, all vesicles surrounded by large vacuoles (Figs 7A-B). The inner surface of the pusule vesicles had a thin coating of parallel fibrilla, giving them a striated appearance (Fig. 7B).

Flagellar apparatus: The basal bodies of the flagella inserted at an angle of about 170°, the basal body of the longitudinal flagellum shifted one basal body width outwards towards the ventral ridge (Fig. 8A-C). Small connectives (bbc) were seen between the two basal bodies (Fig. 8B-C, 9E-F) or connecting to a forming basal body (Fig. 8A-B). The R3 and R4 flagellar roots were attached to the side of the transverse basal body (TB) (Figs 8B, F, 9D), extending along the plasmalemma on opposite sides of the transverse flagellum/pusule canal (Fig. 8J). A small connective (R4/TBc) was present between the R4 and TB (Fig. 9C). The R4 root continued forwards on the ventral side of the cell below the amphiesma, for some distance lining the cingulum (Fig. 8B-E). The transverse microtubular extension (TMRE) of the R3 extended between the two pusules (Figs 7A, 8H). Opaque material of the R1 flagellar root almost enclosed the longitudinal basal body (LB) (Figs 8D, F, 9G-I) and extended downwards towards the sulcus (Figs 8B-E, 9E-I), lining the longitudinal amphiesmal invagination (LAI) (Fig. 9J-K). A striated ventral connective was attached to the ventral side of the R1 a short distance from the LB and extended for a distance of approximately 250 nm before connecting to the topmost part of the LAI (Figs 8I, 9G-I). A broad striated root connective (src) interconnected the R1 and R4 roots (Figs 8D-H, 9E-F). An indistinct R2 root was sometimes seen attached to the LB (Fig. 9I).

Phylogeny

The LSU rDNA sequence of *Kirithra asteri* was compared to an assemblage of other dinoflagellates covering various evolutionary lineages at the level of families and orders (e.g. Kareniaceae, Tovelliaceae, Gonyaulacales, Suessiales, Dinophysiales). In Figure 10 , *K. asteri* forms a sister taxon to *Gymnodinium* sp. 1 (KF245462), but with moderate branch support only (posterior probability in BA = 0.72 and bootstrap support in ML = 68%). *Kirithra* and *Gymnodinium* sp. 1 formed a sister group to a large assemblage comprising *Ceratoperidinium* spp., *Cochlodinium* spp. and *Gymnodinium* sp. 2. The branch support for this part of the tree topology was high in both BA and ML (1.0 and 99%, respectively) indicating that the cluster forms a distinct evolutionary lineage. The resolution of the deep branches was not revealed due to low support values.

Discussion

Identity of the Dinoflagellate

Searching the literature for morphologically similar marine dinoflagellates with a classic gymnodinioid appearance led to a list comprising *Gymnodinium auratum* Kofoid & Swezy, *Gymnodinium maguelonnense* Biecheler, *Gymnodinium ochraceum* Kofoid, *Gyrodinium capsulatum* Kofoid & Swezy, *Gyrodinium foliaceum* Kofoid & Swezy (Biecheler 1952; Kofoid 1931; Kofoid and Swezy 1921) (Fig. 11A-G) and *Gymnodinium bonaerense* Akselman (Akselman 1985) (Fig. 11H). Their overall morphology was comparable to *Kirithra asteri* allowing for small differences in LM (Fig. 1A-I). A drawing of *K. asteri* is included here for comparison (Fig. 12). Two of the species, *Gym. auratum* (Fig. 11A) and *Gyr. capsulatum* (Fig. 11E) could be excluded as they were described as lacking chloroplasts (Kofoid & Swezy 1921). *Gym. ochraceum* (Fig. 11F) and *Gyr. foliaceum* (Fig. 11G) have chloroplasts but there is no description of central pyrenoids and both species are significantly larger than *Kirithra asteri*. *Gym. ochraceum* has a dark-brown colour, a central nucleus, and lacks a sulcal extension (Kofoid 1931). *Gyr. foliaceum* (Fig. 11G),

a large vesicle containing flagellar hairs (fh) is seen to the right of the nucleus. Several peripheral and inwards radiating chloroplasts are visible. **C**) Transverse section of bottom half of hypocone. Nucleus with condensed chromosomes visible in cell centre (N). Numerous small vesicles with electron-opaque centre (seen in detail in F-G) are dispersed in the cytosol and along the amphiesma (arrows). Some of the trichocysts are also indicated (tr). **D-E**) TAI in longitudinal section showing a row of circular microtubules (arrows) supporting the invagination. **F-G**) Higher magnification of electron-dense multi-layered material within vesicles (arrow in Figs 4C, 5C). **H**) Longitudinal and transverse sections of two profiles of longitudinal flagella. Cross-banded "packing material" is found adjacent to axoneme (arrow). A cross-striated muscle-like fibre runs along the axoneme (arrowhead), also seen in cross-section.

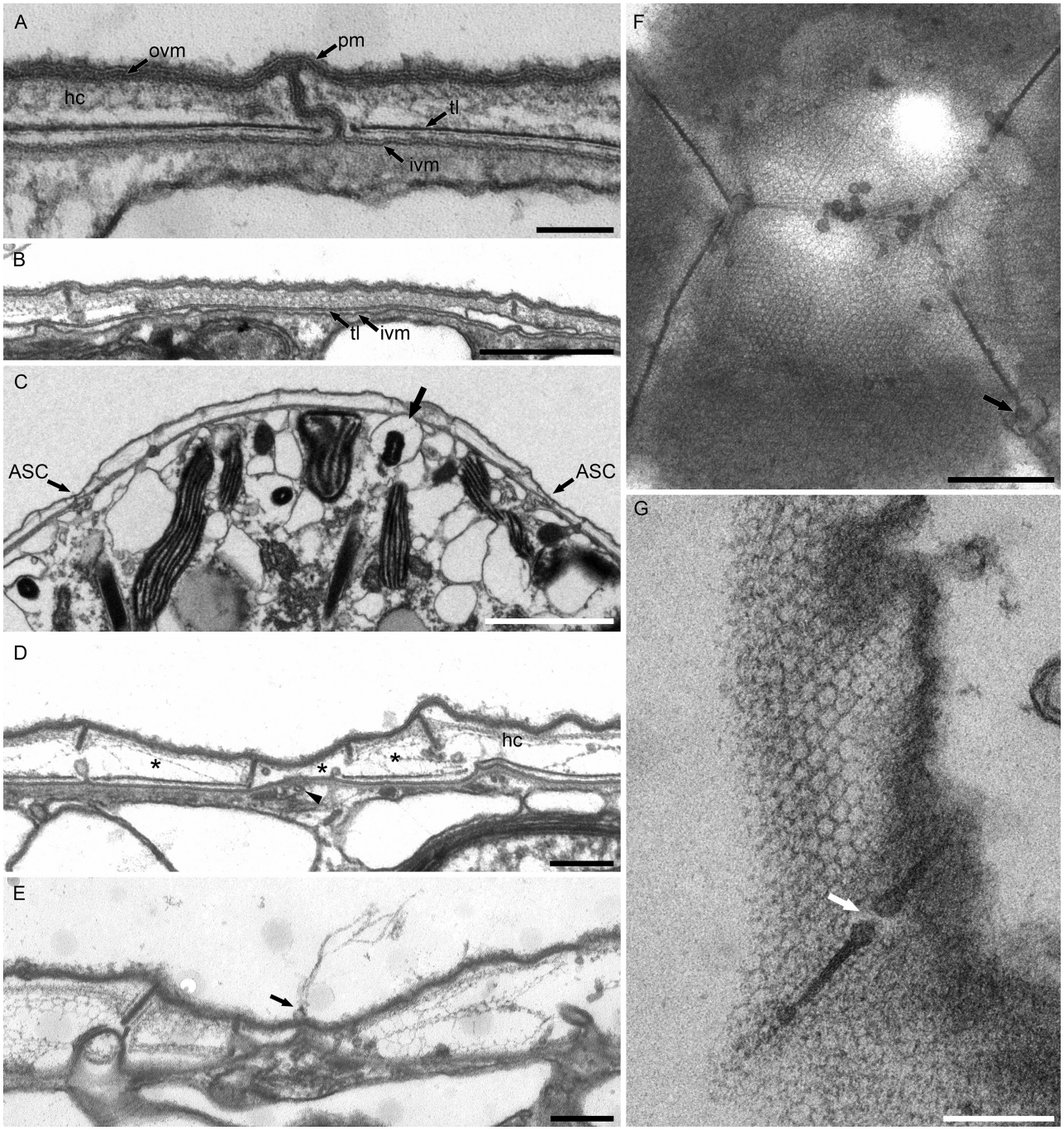

Figure 5. *Kirithra asteri* gen. et sp. nov. TEM, amphiesmal vesicles, trilaminar layer, honeycomb and details of the apical structure complex (ASC). Scale bars: A = 100 nm; B, F = 500 nm; C = 2 μm; D-E, G = 200 nm. **A**) High magnification of two adjoining amphiesmal vesicles, showing outermost continuous plasma membrane (pm), outer amphiesmal vesicle membrane (ovm), inner amphiesmal vesicle membrane (ivm) and within each vesicle, the discontinued trilaminar layer (tl). The honeycomb layer (hc) seen as fibrillar material against ovm. Fixation schedule 1. **B**) Amphiesma with broken amphiesmal vesicle junctions and continuous trilaminar layer (tl). The inner amphiesmal vesicle membranes (ivm) are also continuous. Fixation schedule 2. **C**) Cell apex. Circular apical structure complex (ASC) present subapically on both sides. Vesicles with electron-dense centres visible (arrow). Fixation schedule 1. **D**) ASC at higher magnification showing three amphiesmal vesicles (asterisks). The central vesicle shows an elevation of the cytosol under which a microtubule is present (arrowhead).

on the other hand, has a narrow sulcus and lacks the outer hyaline sheath, called a periplast or hyaline cyst in the other species mentioned above (Kofoid 1931; Kofoid and Swezy 1921). *Gym. maguelonnense* (Figs 11B-D) was described as 34–42 μm long, with chloroplasts, a round apical structure complex and a large nucleus placed at the level of the cingulum. However, the meticulously prepared drawings, replicating the pattern of the amphiesmal vesicles (Fig. 11C), showed a greater amount of amphiesmal vesicles compared to *K. a*steri. Furthermore, the apical structure was ovoid and made an incomplete loop around the apex (Fig. 11D, Biecheler 1952) whereas the ASC of *K. asteri* forms a complete circular loop. The nucleus in *K. asteri* was positioned in the hypocone. *Gymnodinium bonaerense* (Fig. 11H), described by Akselman (1985) from the same area as *Kirithra* differs from *Kirithra* in being smaller, having a round, rather than conical epicone, a centrally located nucleus, and it was described with a circular cingulum (in a personal communication from Rut Akselmann to ØM in May 2017, she mentioned that this species may be conspecific with *Karenia mikimotoi*). Hence, *K. asteri* is considered a distinct, previously unknown species.

A few undescribed dinoflagellates showing significant similarities were also located in the literature. The first potential match was in Omura et al. (2012) and called "*Gymnodinium*" sp.2 (from the Western Pacific). Additional light microscopy images were received from one of the authors (M. Iwataki) and these showed cells that were both identical in size and morphological features (e.g. hyaline amphiesma, nucleus in the hypocone, sulcal extension, irregularly shaped vacuoles and circular ASC). Unfortunately, ultrastructural or phylogenetic information was not available for this material, which may be identical to *Kirithra asteri*. *Kirithra asteri* also appeared to be morphologically similar to *Gymnodinium* sp. 1 and *Gymnodinium* sp. 2 in Reñé et al. (2013) and are also included in our phylogenetic tree. Two SEM pictures were included of *Gymnodinium* sp. 1 in this publication and they are practically identical to our micrographs of *Kirithra asteri* although the cells in the published figures seem to have shrunk slightly. In the phylogenetic tree, this species groups with *Kirithra asteri* (Fig. 10). A single LM picture of *Gymnodinium* sp. 2 was included by Reñé et al. (2013), and although the length of the cell was stated to be 38 μm, our measurements of the cell according to the scale bar, gave a length of approx. 47 μm (Reñé et al. 2013). If the scale bar is correct, then *Gymnodinium* sp. 2 is significantly larger than *Kirithra asteri*. It did not group with *Kirithra* in the phylogenetic tree.

Phylogeny vs. Morphology

In the phylogenetic tree (Fig. 10), *Kirithra asteri* formed a statistically well-supported clade with *Ceratoperidinium* spp., *Cochlodinium* spp. and *Gymnodinium* spp. (posterior probability in BA = 1.0 and bootstrap support in ML = 99%). Dinoflagellates within this clade conform with the few family characteristics of the Ceratoperidiniaceae by being naked, phototrophic and exhibiting a circular apical structure complex (Reñé et al. 2013), although micrographs of the phylogenetically separated *Ceratoperidinium falcatum* (KJ508394) (*Gymnodinium fusus*) have not been published. The generic names *Gymnodinium* and *Cochlodinium* presently ascribed to members of the family, should therefore be modified as discussed by Reñé et al. (2013) and the tree topology indicates the presence of four or five distinct genera belonging to the Ceratoperidiniaceae. Detailed studies of morphology and ultrastructure of the species in this clade are needed to resolve their interrelationship.

Ceratoperidinium margalefii was described as having a theca and a large apical pore, a description copied by Loeblich (1980) from Margalef's original description (Margalef 1969). The same description was applied by Loeblich (1980) to his new family Ceratoperidiniaceae.

Gymnodinium fusus (syn. *Ceratoperidinium falcatum*), however, is naked, without an apical pore but with a circular apical furrow. *Kirithra asteri* also appears naked in the light microscope. However, in this species the cell cytoplasm sometimes retracts slightly from the amphiesma to give the impression of a theca (Fig. 1H-I, K-L). It is possible, therefore, that Margalef (1969) misidentified a theca in *Ceratoperidinium margalefii*, the amphiesma being very thin. Margalef specifically mentions that dis-

The trilaminar layer is absent in the central vesicle. The honeycomb layer seen as filaments (hc). Fixation schedule 1. **E**) High magnification showing mucilaginous material released from central amphiesmal vesicle of ASC (arrow). Fixation schedule 1. **F**) Tangential section of amphiesma showing elaborate honeycomb pattern inside amphiesmal vesicles. Junctions of vesicles and a pore (arrow) is visible. Fixation schedule 2. **G**) High magnification of honeycomb structure within amphiesmal vesicles. Junction between amphiesmal vesicles contains a pore (arrow). Fixation schedule 2.

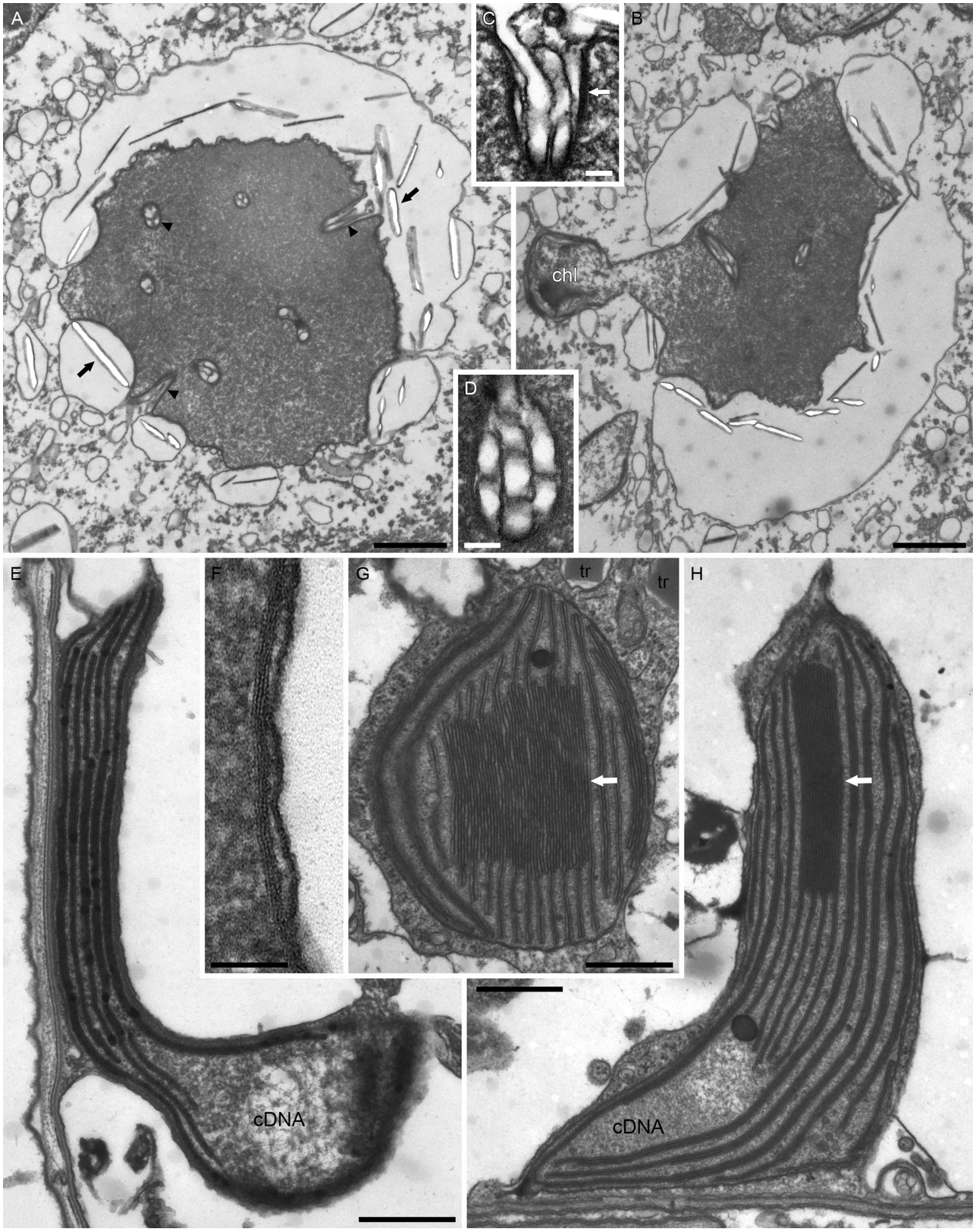

Figure 6. *Kirithra asteri* gen. et sp. nov. TEM, pyrenoids and chloroplasts. Scale bars: A-B = 1 μm, C-D = 100 nm, E = 500 nm, F = 50 nm, G-H = 500 nm. **A**) Pyrenoid with invaginations (arrowheads), surrounded

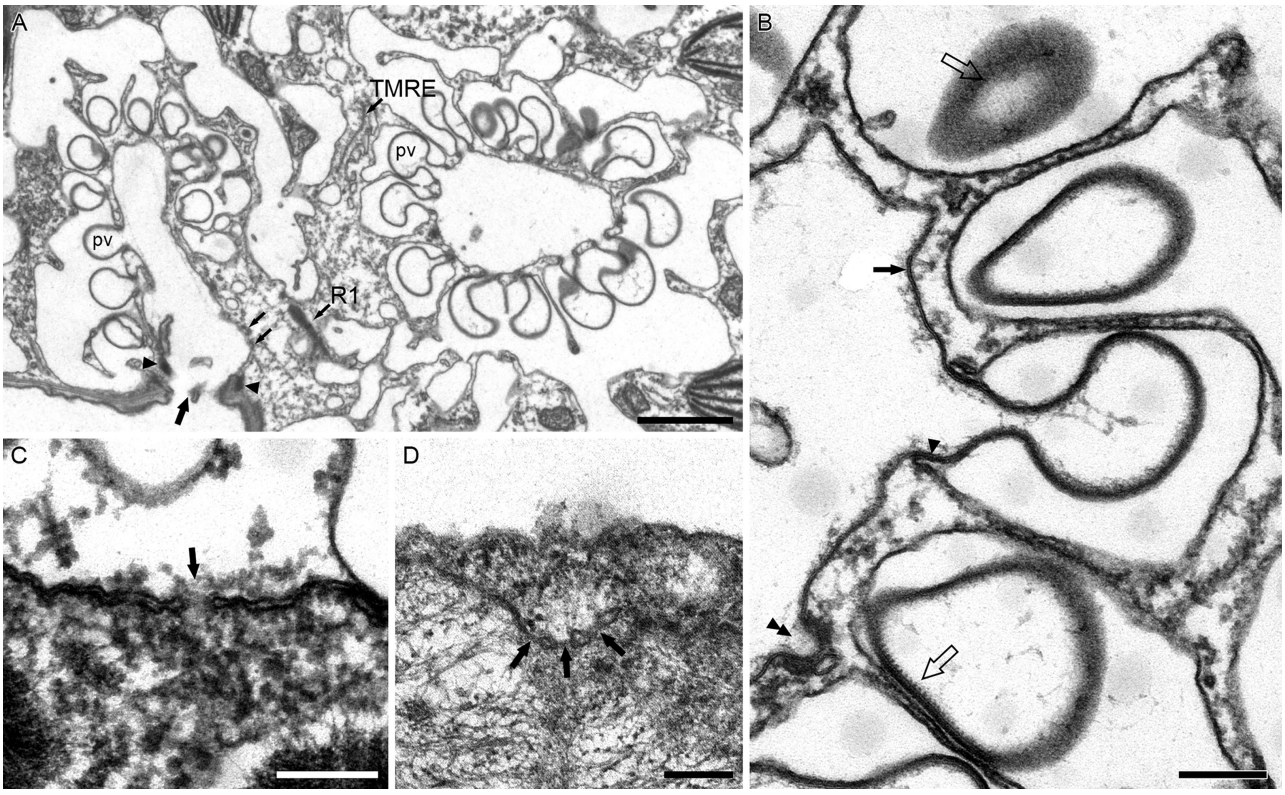

Figure 7. *Kirithra asteri* gen. et sp. nov. TEM, pusules and nuclear pores. Scale bars: A = 1 μm, B-D = 200 nm. **A**) Two pusules with central collecting chamber and associated pusule vesicles (pv) that open into each chamber. All vesicles are surrounded by large vacuoles. The left collecting chamber opens into the flagellar canal and further into the transverse amphiesmal invagination (large arrow). Collared pits (small arrows). Transverse striated collar surrounds the opening of each flagellar canal (arrowheads). R1 flagellar root and transverse microtubular extension (TMRE) visible. Fixation schedule 1. **B**) Higher magnification of pusule vesicles. The single membrane of the collecting chamber (arrow) continues into the pusule vesicles. Each vesicle has a constricted opening connected to the collecting chamber. The vacuolar membrane is tightly appressed to the membrane of the vesicles (arrowhead). Vesicle lumen with thin fibrillar striated coating (open arrows). Constricted opening of a pusule vesicle resembling a collared pit (double arrowhead). Fixation schedule 1. **C**) Nuclear envelope with pore (arrow). Fixation schedule 1. **D**) At least three pores (arrows) assembled in slight invagination in the nuclear envelope. Fixation schedule 2.

tinct amphiesmal plates were not possible to see, and in *Kirithra* very small amphiesmal vesicles could only occasionally be seen in the light microscope.

The genus *Ceratoperidinium* is placed within this well-supported assemblage of the molecular tree, forming a distinct evolutionary lineage away from *K. asteri*, with *Gymnodinium* sp. 1 in a sister group position. Species of *Ceratoperidinium* have also been described to possess retractile appendices during some stages of the life cycle. Different life cycle stages or variations in the morphology such

vesicles containing tile-like inclusions (arrows). Fixation schedule 1. **B**) Pyrenoid with associated radiating chloroplast (chl). Fixation schedule 1. **C**) Higher magnification of invagination into pyrenoid. Four membranes are tightly appressed, one from the vesicle and three from the pyrenoid (arrow). Fixation schedule 1. **D**) Higher magnification of cross-sectioned invagination showing several vesicle membranes within the invagination. Fixation schedule 1. **E**) Peripheral chloroplast with thylakoids in stacks of two to three and area of chloroplast DNA (cDNA). Fixation schedule 1. **F**) Four membranes surround the pyrenoid, one of them probably from a vesicle. Fixation schedule 1. **G-H**) Chloroplasts with granum-like stacks of thylakoids (arrows). Two trichocysts (tr) are visible in Figure 6G and an area of chloroplast DNA is visible in Figure 6H (cDNA). Note two trichocysts (tr) in Figure 6G. Fixation schedule 2.

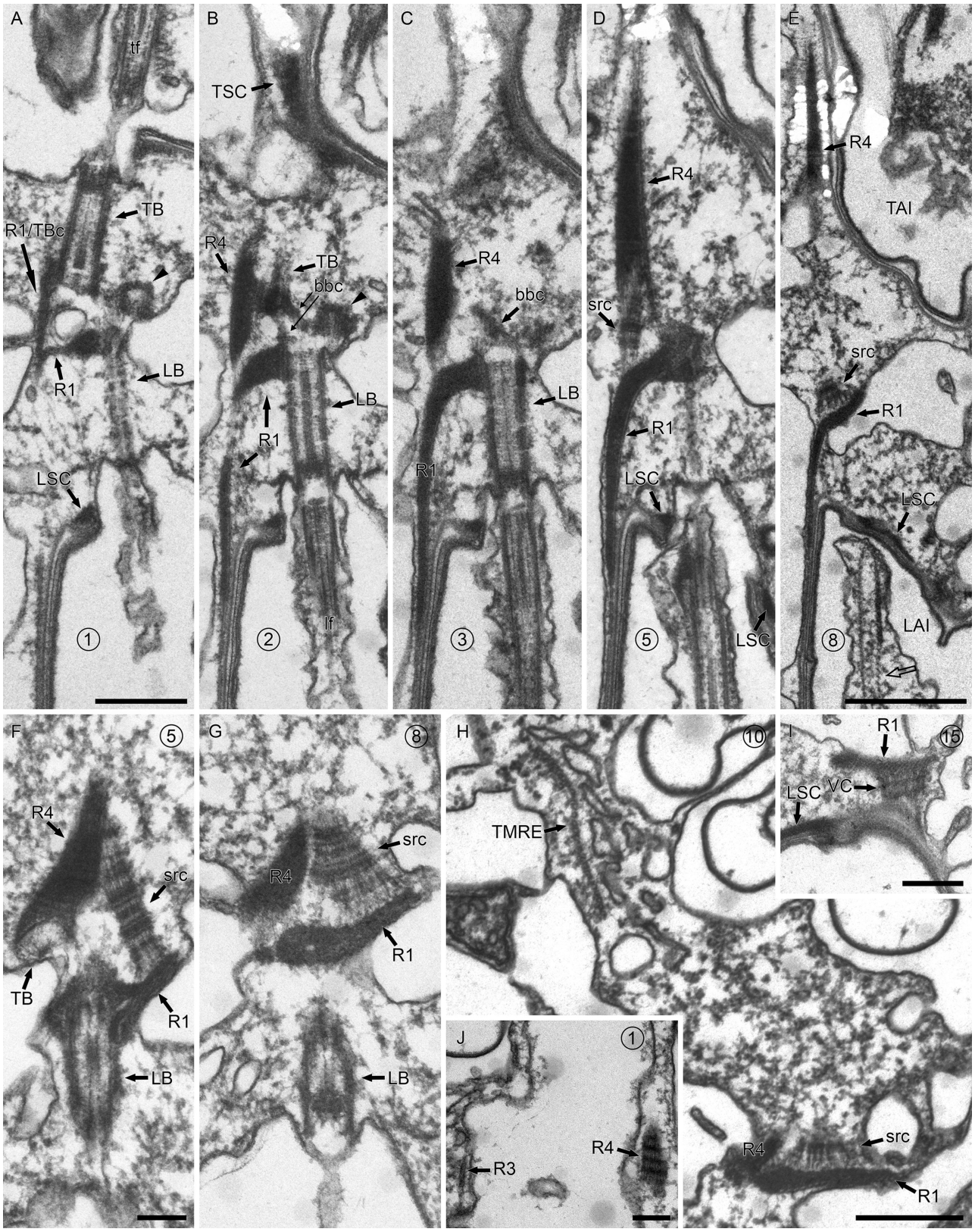

Figure 8. *Kirithra asteri* gen. et sp. nov. Non-adjacent serial sections showing flagellar apparatus (FA). Encircled numbers represent section numbers. Fixation schedule 1. Scale bars: A-D, H-I = 500 nm, E = 1 μm,

as retractility of the cell were not observed in *K. asteri* (nor in *Gymnodinium* sp. 1, Reñé et al. 2013). This combination of features leads to conclude that *K. asteri* is a distinct genus rather than a species of *Ceratoperidinium*.

Kirithra asteri formed a sister taxon to the morphologically similar *Gymnodinium* sp. 1 and to ensure that the divergence between the two was not due to different sequence lengths, a sequence comparison based on 811 base pairs including the variable D2 domain was done. It gave a p-distance of 6.3%, the two taxa differing in 52 of 811 base pairs. This divergence value indicates that *K. asteri* and *Gymnodinium* sp. 1 sensu Reñé et al. (2013) are different species despite the two resembling each other in SEM. It stresses the need for a detailed ultrastructural study of *Gymnodinium* sp. 1 which is probably a second species of *Kirithra*.

Ultrastructure

The present study is the first containing ultrastructure of a species within Ceratoperidiniaceae, and several interesting features were observed. Some of these are discussed below.

The apical structure complex (ASC) is now widely used when classifying naked dinoflagellates (Daugbjerg et al. 2000, Moestrup and Daugbjerg 2007). Within the last few years at least 15 ASCs of different genera have been described (Boutrup et al. 2016; Gómez et al. 2015; Hansen and Daugbjerg 2011; Hoppenrath et al. 2012; Jang et al. 2017; Jeong et al. 2014; Kang et al. 2011; Moestrup et al. 2014; Reñé et al. 2013; Sampedro et al. 2011; Takano et al. 2014; Yamada et al. 2013; Yuasa et al. 2016), while two genera (*Asulcocephalium* and *Leiocephalium*) have been found to lack an ASC (Takahashi et al. 2015). In three of the genera the ASC forms a complete circle. The ASC of the closest relative to *K. asteri*, *Ceratoperidinium* (Reñé et al. 2013), was described only three months after the first circular ASC was observed in the genus *Bispinodinium* Yamada & Horiguchi (Yamada et al. 2013). A second species with a circular ASC, *Cucumeridinium* Goímez, Loípez-Garciía, Takayama & Moreira, was found two years later (Goímez et al. 2015). The morphological differences of the three genera are profound, and the phylogenetic analysis of LSU rDNA did not reveal any phylogenetic relationship between *Ceratoperidinium* and *Bispinodinium*. Unfortunately, LSU rDNA data are not available for *Cucumeridinium*, but the SSU rDNA phylogeny provided by Goímez et al. (2015) showed *Cucumeridinium* as a sister taxon to a clade containing e.g. *Alexandrium* Halim, *Gonyaulax* Diesing, and *Protoceratium* Bergh (support value PP = 0.77), none of which are closely related to *Ceratoperidinium* or *Bispinodinium* in the LSU rDNA phylogeny (Fig. 10). Thus, seemingly identical circular ASCs have evolved more than once in the evolutionary history of dinoflagellates. It is not known whether all ASCs have the same detailed structure, as ultrastructural investigations are missing. The circular ASC of *K. asteri*, (Fig. 13) and therefore perhaps of all members of the family Ceratoperidiniaceae, consists of three parallel series of vesicles, the central one with knobs. The microtubule present below the central vesicle of the ASC may be homologous with the single microtubule found to support the groove in *Akashiwo sanguinea* (Hirasaka) Hansen & Moestrup (Daugbjerg et al. 2000; Roberts and Roberts 1991, figs 9, 11).

Amphiesma: An elaborate polygonal honeycomb layer was found within the amphiesmal vesicles of *K. asteri* and was most apparent when sectioned tangentially (Fig. 5F-G). Schematic drawings of the polygonal honeycomb layer is included as Figure 14. Such a structure has been described previously in *Gymnodinium cryophilum* (Wede-

F-G, J = 200 nm. **A-E**) FA of cell in Figure 4B, ventral side to the right, dorsal side to the left. **A**) Transverse basal body (TB) at about 170° angle to longitudinal basal body (LB). Flagellar root (R1). A connective (R1/TBc) is visible between R1 and TB. Transverse flagellum (tf) and longitudinal striated collar (LSC). Forming basal body (arrowhead). **B-C**) Small basal body connectives (bbc), one between TB and LB, and one between TB and a forming basal body (arrowhead). R1 flagellar root connects to LB, and R4 root to TB. Transverse striated collar (TSC) and longitudinal flagellum (lf) visible. **D**) Striated root connective (src) present between R1 and R4. The LSC is visible on both sides of the flagellar pore. **E**) Lower magnification showing R4 continuing upwards and R1 downwards from the src. LSC in tangential section and cross-hatched "packing" material associated with the longitudinal flagellum visible (open arrow). Transverse and longitudinal amphiesmal invaginations visible (TAI and LAI). **F-J**) FA of cell in Figure 4A. **F-G**) TB and LB with associated striated roots R4 and R1 respectively, connected by src. **H**) Lower magnification also showing the transverse microtubular extension (TMRE). **I**) Ventral connective (VC) running from R1 to amphiesma in topmost part of the longitudinal amphiesmal invagination. LSC in tangential section. **J**) Single microtubule of the R3 and striated root R4 on each side of pusule canal connected to the transverse flagellar canal.

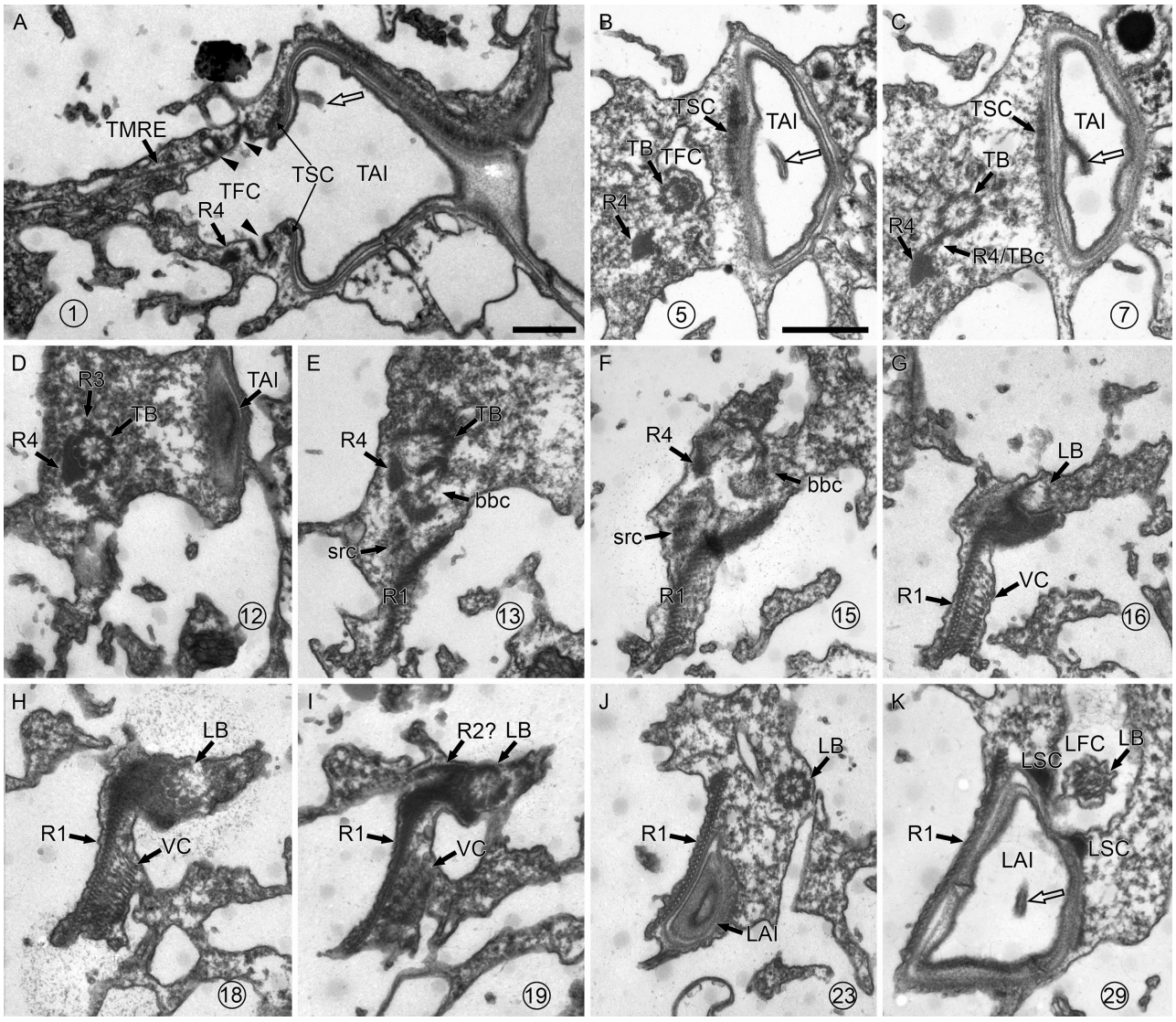

Figure 9. *Kirithra asteri* gen. et sp. nov. TEM showing flagellar apparatus of cell in transverse section. Non-adjacent serial sections, proceeding from the top of the cell downwards, ventral side to the right. Encircled numbers represent section numbers. Fixation schedule 1. Scale bars: 500 nm. **A**) Triangular transverse amphiesmal invagination (TAI), separated from the transverse flagellar canal (TFC), by the transverse striated collar (TSC). Transverse microtubular extension (TMRE) and R4 present on each side of the canal. Collared pits (arrowheads) are also present. A flap protrudes into the TAI (open arrow). **B**) Transverse basal body (TB) next to TFC, and R4 within the TSC. TAI with protruding flap (open arrow). **C**) TB with connective to R4 (R4/TBc). Tangential section of TSC. TAI with protruding flap (open arrow). **D**) TB with R4 and transverse section of R3 microtubule. Tangential section of TAI. **E**) Basal body connective (bbc) and striated root connective (src) between R1 and R4 visible. **F**) Another bbc and more pronounced src between R1 and R4. **G-H**) Longitudinal basal body (LB) connected to R1. Ventral connective (VC) attached to ventral side of R1. **I**) Single microtubule (R2?) running from LB next to the R1 with VC. **J**) R1 consisting of app. 34 microtubules besides the longitudinal amphiesmal invagination (LAI). **K**) Longitudinal striated collar (LSC) separating LFC and LB from LAI, also exhibiting a protruding flap (open arrow). R1 lining LAI.

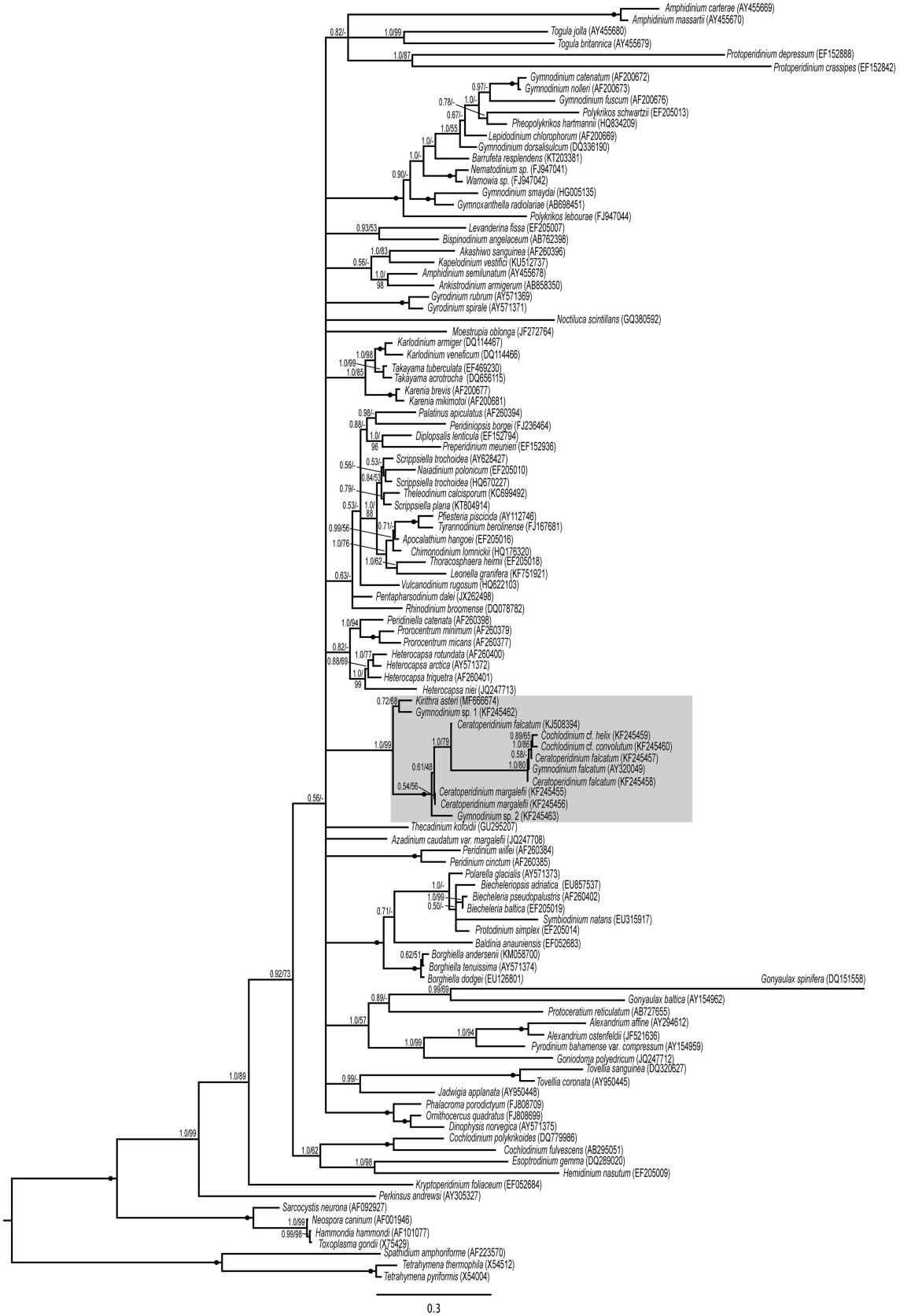
Amphidinium carterae (AY455669)
Amphidinium massartii (AY455670)
Togula jolla (AY455680)
Togula britannica (AY455679)
Protoperidinium depressum (EF152888)
Protoperidinium crassipes (EF152842)
Gymnodinium catenatum (AF200672)
Gymnodinium nolleri (AF200673)
Gymnodinium fuscum (AF200676)
Polykrikos schwartzii (EF205013)
Pheopolykrikos hartmannii (HQ834209)
Lepidodinium chlorophorum (AF200669)
Gymnodinium dorsalisulcum (DQ336190)
Barrufeta resplendens (KT203381)
Nematodinium sp. (FJ947041)
Warnowia sp. (FJ947042)
Gymnodinium smaydai (HG005135)
Gymnoxanthella radiolariae (AB698451)
Polykrikos lebourae (FJ947044)
Levanderina fissa (EF205007)
Bispinodinium angelaceum (AB762398)
Akashiwo sanguinea (AF260396)
Kapelodinium vestifici (KU512737)
Amphidinium semilunatum (AY455678)
Ankistrodinium armigerum (AB858350)
Gyrodinium rubrum (AY571369)
Gyrodinium spirale (AY571371)
Noctiluca scintillans (GQ380592)
Moestrupia oblonga (JF272764)
Karlodinium armiger (DQ114467)
Karlodinium veneficum (DQ114466)
Takayama tuberculata (EF469230)
Takayama acrotrocha (DQ656115)
Karenia brevis (AF200677)
Karenia mikimotoi (AF200681)
Palatinus apiculatus (AF260394)
Peridiniopsis borgei (FJ236464)
Diplopsalis lenticula (EF152794)
Preperidinium meunieri (EF152936)
Scrippsiella trochoidea (AY628427)
Naiadinium polonicum (EF205010)
Scrippsiella trochoidea (HQ670227)
Theleodinium calcisporum (KC699492)
Scrippsiella plana (KT804914)
Pfiesteria piscicida (AY112746)
Tyrannodinium berolinense (FJ167681)
Apocalathium hangoei (EF205016)
Chimonodinium lomnickii (HQ176320)
Thoracosphaera heimii (EF205018)
Leonella granifera (KF751921)
Vulcanodinium rugosum (HQ622103)
Pentapharsodinium dalei (JX262498)
Rhinodinium broomense (DQ078782)
Peridiniella catenata (AF260398)
Prorocentrum minimum (AF260379)
Prorocentrum micans (AF260377)
Heterocapsa rotundata (AF260400)
Heterocapsa arctica (AY571372)
Heterocapsa triquetra (AF260401)
Heterocapsa niei (JQ247713)
Kiritthra asteri (MF666674)
Gymnodinium sp. 1 (KF245462)
Ceratoperidinium falcatum (KJ508394)
Cochlodinium cf. helix (KF245459)
Cochlodinium cf. convolutum (KF245460)
Ceratoperidinium falcatum (KF245457)
Gymnodinium falcatum (AY320049)
Ceratoperidinium falcatum (KF245458)
Ceratoperidinium margalefii (KF245455)
Ceratoperidinium margalefii (KF245456)
Gymnodinium sp. 2 (KF245463)
Thecadinium kofoidii (GU295207)
Azadinium caudatum var. margalefii (JQ247708)
Peridinium willei (AF260384)
Peridinium cinctum (AF260385)
Polarella glacialis (AY571373)
Biecheleriopsis adriatica (EU857537)
Biecheleria pseudopalustris (AF260402)
Biecheleria baltica (EF205019)
Symbiodinium natans (EU315917)
Protodinium simplex (EF205014)
Baldinia anauniensis (EF052683)
Borghiella andersenii (KM058700)
Borghiella tenuissima (AY571374)
Borghiella dodgei (EU126801)
Gonyaulax spinifera (DQ151558)
Gonyaulax baltica (AY154962)
Protoceratium reticulatum (AB727655)
Alexandrium affine (AY294612)
Alexandrium ostenfeldii (JF521636)
Pyrodinium bahamense var. compressum (AY154959)
Goniodoma polyedricum (JQ247712)
Tovellia sanguinea (DQ320627)
Tovellia coronata (AY950445)
Jadwigia applanata (AY950448)
Phalacroma porodictyum (FJ808709)
Ornithocercus quadratus (FJ808699)
Dinophysis norvegica (AY571375)
Cochlodinium polykrikoides (DQ779986)
Cochlodinium fulvescens (AB295051)
Esoptrodinium gemma (DQ289020)
Hemidinium nasutum (EF205009)
Kryptoperidinium foliaceum (EF052684)
Perkinsus andrewsi (AY305327)
Sarcocystis neurona (AF092927)
Neospora caninum (AF001946)
Hammondia hammondi (AF101077)
Toxoplasma gondii (X75429)
Spathidium amphoriforme (AF223570)
Tetrahymena thermophila (X54512)
Tetrahymena pyriformis (X54004)
0.3

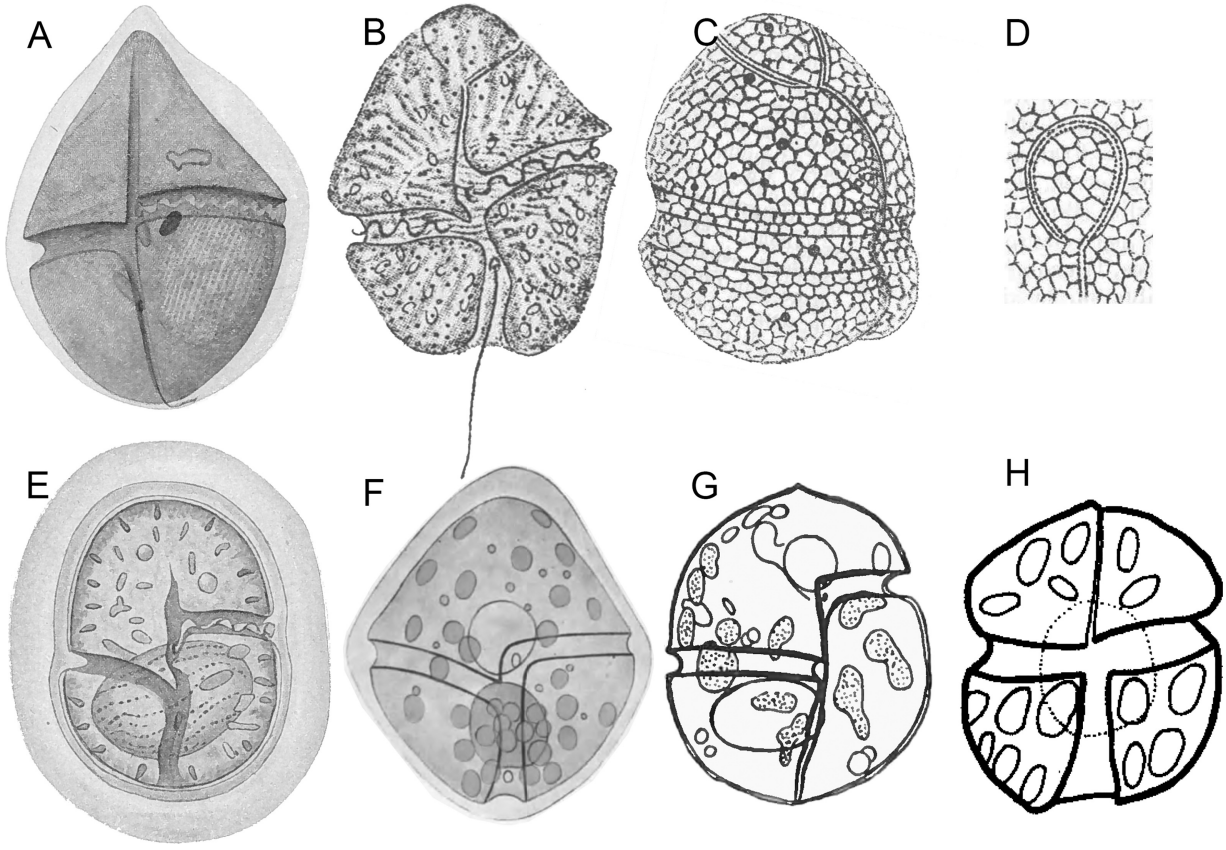

Figure 11. Original illustrations of species similar to *Kirithra asteri*. No scale bars provided. **A**) *Gymnodinium auratum*, reproduced from Kofoid & Swezy (1921, pl. 2, fig. 20). **B-D**) *Gymnodinium maguelonnense*, reproduced from Biecheler (1952, fig. VIII, 1-3). **B**) Live cell. **C**) Amphiesmal tabulation. **D**) Apical structure complex. **E**) *Gyrodinium capsulatum*, Kofoid & Swezy (1921, pl. 5, fig. 54). **F**) G*ymnodinium ochraceum*, reproduced from Kofoid (1931, pl. 1, Fig. 6). **G**) *Gyrodinium foliaceum*, reproduced from Kofoid & Swezy (1921, text fig. CC, fig. 18). **H**) *Gymnodinium bonaerense* reproduced from Akselman (1985, fig. 5).

mayer, Wilcox & Graham) Hansen & Moestrup (as *Amphidinium*, Wilcox et al. 1982), *Nusuttodinium poecilochroum* (Larsen) Takano & Horiguchi (as *Amphidinium*, Larsen 1988), *Noctiluca scintillans* (Macartney) Kofoid & Swezy (as *N. miliaris*, Melkonian and Höhfeld 1988), and in *Gyrodinium spirale* (Bergh) Kofoid & Swezy (Hansen and Daugbjerg 2004). In *Heterocapsa niei* (Loeblich III) Morrill & Loeblich III the honeycomb was found as a "precipitate" on what was called the pellicular layer (Höhfeld and Melkonian 1992). Since none of these species are closely related to each other, a honeycomb structure may be more widespread in dinoflagellates, as suggested by Larsen (1988). When sectioned at certain angles, or in poorly preserved vesicles, the honeycomb becomes more or less fibrous (Fig. 5A-E). It then resembles material in otherwise empty vesicles of some naked dinoflagellates (e.g. Hansen et al. 2000; Moestrup et al. 2009; Sparmann et al. 2008; Yamada et al. 2013).

Many pores were present on the surface of the amphiesma in *Kirithra asteri*, which is not uncommon in dinoflagellates. However, the location of

Figure 10. Phylogeny of *Kirithra asteri* gen. et sp. nov. and a diverse assemblage of other dinoflagellates. In total 1481 base pairs (including introduced gaps) of the nuclear-encoded LSU rDNA were analysed using BA. The outgroup taxa comprised ciliates, apicomplexans and *Perkinsus*. Numbers before slashes are posterior probabilities (≥0.5) from BA followed bootstrap values (≥50%) from ML with 500 replications. The highest possible branch support values in BA and ML (1.0 and 100%, respectively) are indicated by filled circles. GenBank accession numbers are provided in brackets. The lineage encompassing *K. asteri* is marked in grey.

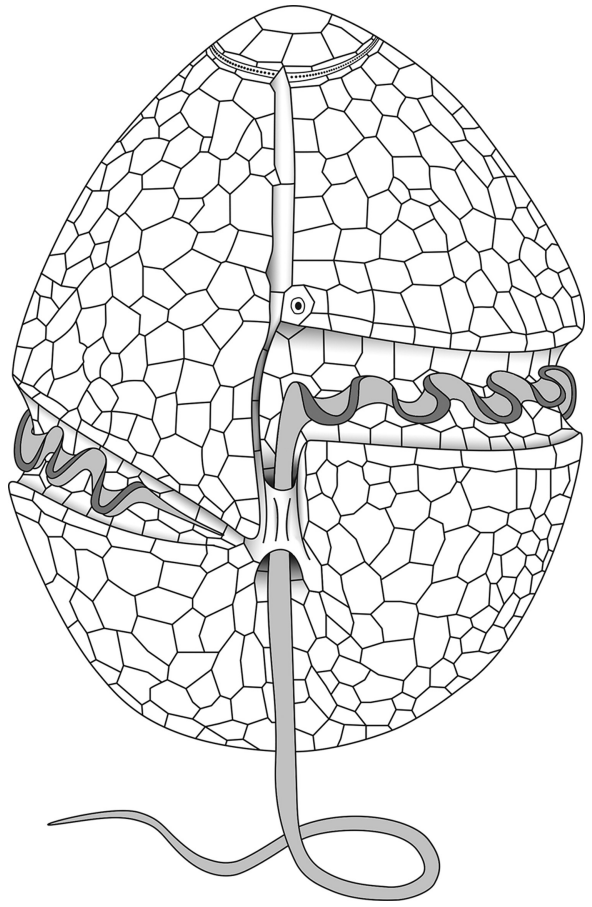

Figure 12. Line drawing of *Kirithra asteri* gen. et sp. nov. based on information obtained from light and scanning electron microscopy.

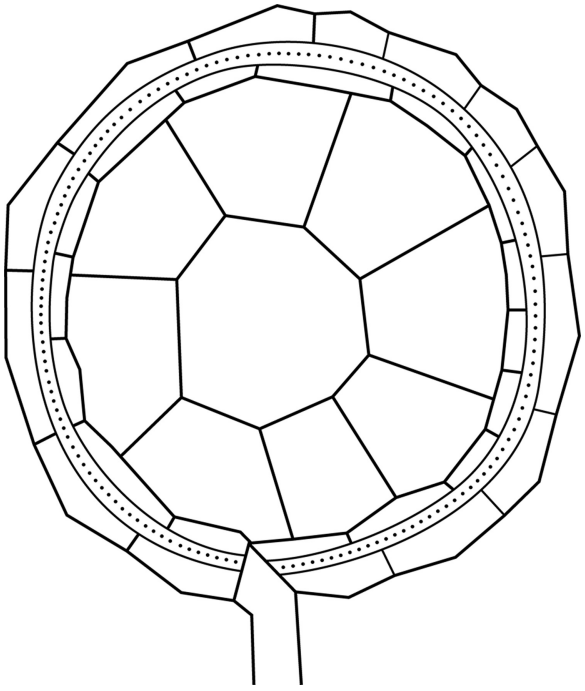

Figure 13. Apical structure complex in *Kirithra asteri* forming a complete circle. The circle is comprised of three rows of vesicles.

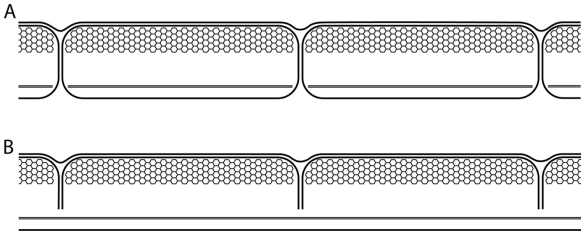

Figure 14. Amphiesma vesicles of *Kirithra asteri*. **A**) Honeycomb structures in the upper part of each of the amphiesma vesicles, and the trilaminar plate-like structure in the lower part of the vesicles. **B**) All trilaminar structures have fused to form a single plate-like structure around the cell, subtended by the fused inner membrane of the amphiesmal vesicles.

the pores, exclusively in the junctions between the amphiesmal vesicles, is not common. *Gyrodiniellum shiwhaense* Kang, Jeong & Moestrup (Kang et al. 2011) appears to possess pores in the junctions but this is hard to determine conclusively from the SEM pictures provided. Contrary to this, *Paragymnodinium shiwhaense* Kang, Jeong, Moestrup & Shin (Kang et al. 2010) possessed very distinct pores in the junctions.

The hyaline amphiesma seems to be shared by all members of Ceratoperidiniaceae studied so far (Reñé et al. 2013).

Trilaminar layer: The appearance of the amphiesma in *K. aste*ri was variable. In some cases, the amphiesmal vesicles were intact, containing the honeycomb and the trilaminar layer, and the vesicles were overlain by a continuous plasma membrane (Fig. 14A). In other cases, the junctions of the amphiesmal vesicles were broken and the honeycomb and junctions stuck to the outer amphiesmal vesicle membrane and the plasma membrane, whereas the trilaminar layer and the underlying inner amphiesmal vesicle membrane both formed a continuous layer around the cell (Fig. 14B). The trilaminar layer was present in all the cells studied. The amphiesma of dinoflagellates has been discussed at length (Bricheux et al. 1992; Calado and Moestrup 2002; Dürr 1979; Höhfeld and Melkonian 1992; Morrill 1984; Morrill and Loeblich 1981; Morrill and Loeblich 1983), and structures resembling the trilaminar layer in *K. asteri* have here been variously described as

a membrane, a pellicle, a dark-staining layer, or a wall. It is difficult to ascribe the trilaminar layer to any of these terms.

Pyrenoid: The pyrenoid(s) is one of the most unusual features of *Kirithra asteri*. Between one and three multiple-stalked invaginated pyrenoids of varying sizes were observed centrally in the cell, and they were visible in the light microscope as circular organelles outlined by refractive material (Fig. 1F-G). Previously, several pyrenoids have been described as multiple-stalked, e.g. in *Amphidinium operculatum* var. *gibbosum* Maranda & Shimizu, *Amphidinium carterae* Hulburt, *Scrippsiella minima* Gao & Dodge, *Scrippsiella acuminata* (Ehrenberg) Kretschmann, Elbrächter, Zinssmeister, Soehner, Kirsch, Kusber & Gottschling, and *Pileidinium ciceropse* Tamura & Horiguchi (Dodge and Crawford 1968, 1971; Gao and Dodge 1991; Maranda and Shimizu 1996; Tamura and Horiguchi 2005). Besides being multiple-stalked, some species also feature different degrees of cytoplasmic invaginations e.g. *Asulcocephalium miricentonis* Takahashi, Moestrup & Iwataki, *Heterocapsa triquetra* (Ehrenberg) Stein, *Palatinus apiculatus* (Ehrenberg) Craveiro, Calado, Daugbjerg & Moestrup, and *Testudodinium maedaense* Katsumata & Horiguchi (Craveiro et al. 2009; Dodge and Crawford 1971; Horiguchi et al. 2012; Takahashi et al. 2015). In *K. asteri* the pyrenoids are multiple-stalked and with invaginations. The pyrenoid matrix is penetrated by membrane-bound extensions from vesicles surrounding the pyrenoids, and these vesicles contain tile-like elements. Multiple finger-like extensions of the vesicles are present in each of the invaginations, forming a regular pattern here (Fig. 6D). This type of invagination has not been reported before. The origin of the tile-like elements is unknown.

Chloroplasts: Dinoflagellates possess chloroplasts lined by different numbers of membranes (e.g. Schnepf and Elbrächter 1999) and the three membranes lining the chloroplast of *Kirithra* indicate that the primary accessory pigment of the plastid is peridinin. To determine the origin of the chloroplasts, analysis of the pigment profile and sequencing of the chloroplast DNA are needed. The chloroplasts displayed large areas of DNA (Fig. 6E, H), which were visible also in the DAPI-stained epifluorescence images (Fig. 1M, O), appearing as blue dots associated with the red chloroplasts.

Grana: Two different TEM fixation schedules were used. Fixation schedule 1 (used on one strain) resulted in 78 serial sections of four cells, and all chloroplasts sectioned had typical distribution of the thylakoids; 2-3 together. In fixation schedule 2 (used on the other strain), about 10 sections each with approximately 15 cells were studied and most chloroplasts exhibited extensive grana formation of the thylakoids, up to 45 thylakoids grouped together (Fig. 6G). The two strains were 100% identical in LSU rDNA sequences. This variability within the same species is very unusual, while grana formation as such has been reported in a large number of dinoflagellate species (Table 1), dispersed throughout the phylogenetic tree. Dodge (1968) reflected that deep stacks of thylakoids might emerge as a result of suboptimal growth conditions, and he generally found grana in old cultures. In the present study, the cultures were kept under the same light and temperature conditions, and were given fresh medium at the same time. Whether the difference found is a strain difference or whether it reflects different physiological states of the two cultures is unknown. Unfortunately, the cultures were subsequently lost and this question must therefore remain open. At the time of fixation, the culture of the strain with the grana was much denser than the strain in which no grana were seen. As the strains had identical nuclear-encoded LSU genes, variations not expressed in the gene sequences may have resulted in grana formation in one but not the other strain. Based on present evidence, the presence of grana is apparently a feature of less taxonomic importance in dinoflagellates than usually thought.

Pusule: The pusules of *K. asteri* were very similar to those of *Amphidinium herdmanii* Kofoid & Swezy (Dodge 1972), *Gymnodinium aureolum* Hulburt (as *Gyrodinium*, Kite and Dodge 1988), *Nusuttodinium poecilochroum* (Larsen 1988), *Takayama xiamenensis* Gu (Gu et al. 2013) and to one of the two dissimilar pusules in *Sphaerodinium cracoviense* Wołoszyńska (Craveiro et al. 2010). Pusules open into the flagellar canals (Fig. 7A) and in the present case the collecting chamber continued directly into the flagellar canals (Fig. 7A).

Vesicles with electron-dense centre: Cells contained numerous membrane-bound vesicles with electron-dense multi-layered material in a concentric pattern. The thickness of one layer was 8–9 nm, which equals the thickness of one of the membranes of the plasma- or amphiesma vesicles. Similar vesicles with membrane-like structures have been found in the parasitic dinoflagellate *Piscinoodinium pillulare* (Schäperclaus) Lom, in *Margalefidinium polykrikoides* (Margalef) Gomez, Richlen & Anderson and in *Barrufeta resplendens* (Hulburt) Gu, Luo & Mertens (Gu et al. 2015; Iwataki et al. 2010; Lom and Schubert 1983). The multi-layered vesicles of *K. asteri* were gen-

Table 1. List of dinoflagellate species reported to contain grana.

Species	References
Alexandrium pseudogonyaulax (Biecheler) Horiguchi ex Kita & Fukuyo	Dodge (1975), as *Goniodoma*
Ansanella granifera Jeong, Jang, Moestrup & Kang	Jeong et al. (2014)
Aureodinium pigmentosum Dodge	Dodge (1967)
Dissodinium lunula (Schütt) Klebs	Dodge (1975), as *Pyrocystis*
Gonyaulax spinifera (Claparède & Lachmann) Diesing	Hansen et al. (1996)
*Gyrodinium dorsu*m Kofoid & Swezy	Dodge (1975)
Leiocephalium pseudosanguineum Takahashi, Moestrup & Iwataki	Takahashi et al. (2015)
Piscinoodinium pillulare (Schäperclaus) Lom	Lom and Schubert (1983)
Protoceratium reticulatum (Claparède & Lachmann) Bütschli	Gaudsmith and Dawes (1972)
Pyramidodinium atrofuscum Horiguchi & Sukigara	Horiguchi and Sukigara (2005)
Scrippsiella minima Gao & Dodge	Gao and Dodge (1991)
Theleodinium calcisporum Craveiro, Pandeirada, Daugbjerg, Moestrup & Calado	Craveiro et al. (2013)

erally associated with the amphiesma, but it was unclear whether the contents were targeting the amphiesma or were to be excreted to the outside of the cell. There was always at least one amphiesmal membrane between the vesicles and the cell exterior.

Ventral pore: The ventral pore (Fig. 2A, F) was a constant feature on the SEM images of *K. asteri*, and low magnification TEM sections of the area of one cell indicated the presence of a superficial invagination of the amphiesma in the same area (not shown). Ventral pores are well known from several armoured dinoflagellate genera like *Alexandrium* and *Azadinium* Elbrächter & Tillmann (Hansen et al. 2003; Tillmann et al. 2010). However, in the naked dinoflagellates ventral pores have only been found in *Karlodinium* Larsen and *Takayama* de Salas, Bolch, Botes & Hallegraeff (Bergholtz et al. 2005; Gu et al. 2013; de Salas et al. 2003, 2008). The ventral pore in *Karlodinium* and *Takayama* is an elongate slit, deeply inserted in the cell, while the pore in *K. asteri* is elliptical to round and positioned at the level of the amphiesma. As TEM showed only a slight invagination, it indicates, together with the fact that the molecular phylogeny separated the two groups, that the pores in the two groups may not be homologous.

Flagellar apparatus: Overall the flagellar apparatus of *Kirithra asteri* consisted of typical flagellar roots, collars, and connectives. A schematic drawing is shown in Figure 15. One rather unusual feature is the ventral connective between the ventral side of the R1 root and the topmost part of the longitudinal amphiesmal invagination. Similar ventral connectives have been found in *Lepidodinium chlorophorum* (Elbrächter & Schnepf) Hansen, Botes & de Salas (as *Gymnodinium*, Hansen and Moestrup 2005), *Margalefidinium polykrikoides* (as *Cochlodinium*, Iwataki et al. 2010), *Levanderina fissa* (Levander) Moestrup, Hakanen, Hansen, Daugbjerg & Ellegaard (Moestrup et al. 2014), *Akashiwo sanguinea* (as *Gymnodinium*, Roberts and Roberts 1991) and in *Woloszynskia limnetica* Bursa, forming a "fibrous connective" between the R1 and the ventral ridge (Roberts et al. 1995). A new basal body was seen forming next to the transverse flagellum with a connective between the two (Figs 8A-B), somewhat like the connective described by Moestrup et al. (2009). The almost opposite orientation of the basal bodies is unusual in dinoflagellates, but seen also in *Karlodinium veneficum* (Ballantine) Larsen (Bergholtz et al. 2005). The longitudinal flagellum contained both cross-hatched "packing material" and a muscle-like striated fibre, previously found in *Tripos muelleri* Bory (as *Ceratium tripos*), *Amphidinium carterae*, *Oxyrrhis marina* Dujardin, *Karlodinium veneficum* and *Nusuttodinium poecilochroum* (Bergholtz et al. 2005; Dodge and Crawford 1968; Larsen 1988; Maruyama 1982; Moestrup 1982).

In conclusion, the study reported here has supported that Ceratoperidiniaceae is a distinct family, and that the new genus and species *Kirithra asteri* is included therein. Additional morphological and ultrastructural information on the closest relatives in the family is required to fully identify the synapomorphic characters of the group.

Methods

Culture: The species was collected during a Rincon area cruise in the Argentine Sea (South Atlantic Ocean) on board the research vessel Dr Bernardo Houssay on September 9th, 2015 (Fig. 16). Two clonal cultures were established

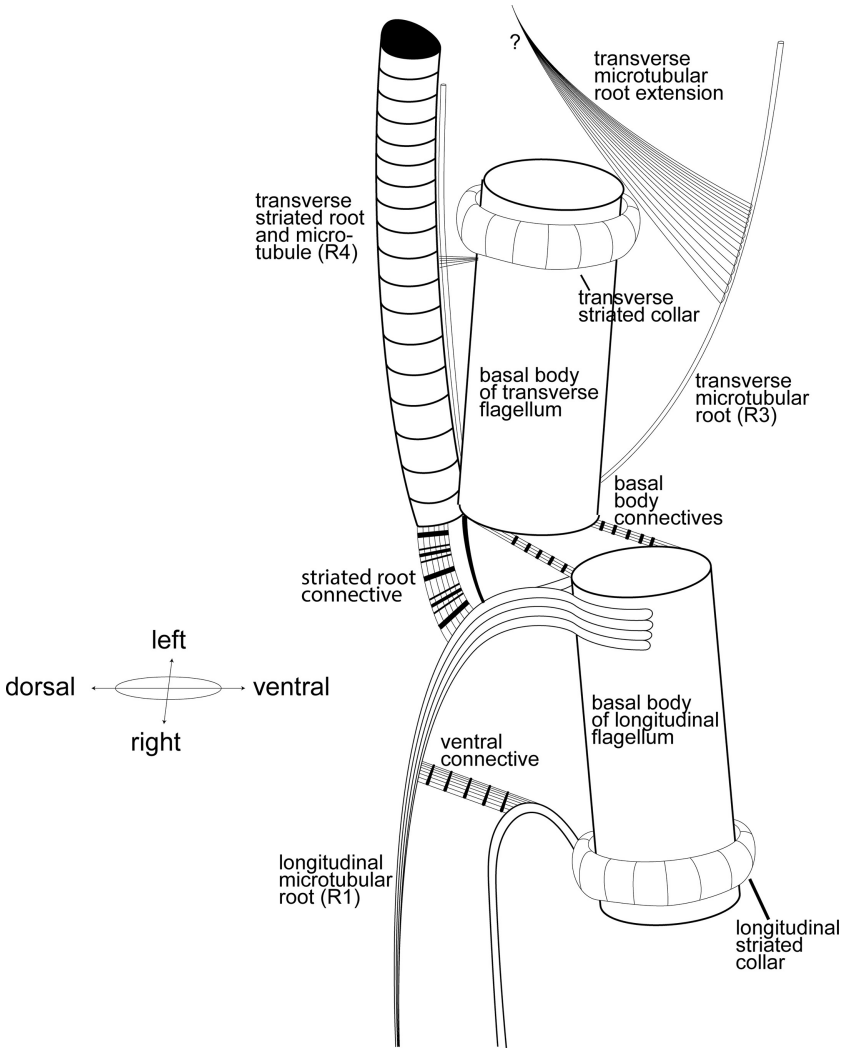

Figure 15. Diagrammatic illustration of the flagellar apparatus in *Kirithra asteri*. The question mark indicates uncertainties about the distal part of the transverse microtubular root extension.

from two single cells, isolated from a CTD bottle collected from 5 meters depth (water temperature 7.2 °C, salinity 33.71, 41°10′48″S 57°51′36″W). The algae were grown in L1 medium (Guillard and Hargraves 1993) without silicate, based on filtered seawater with a salinity of 30 in 50-ml plastic culture flasks at ~50 μmol m^{-2} s^{-1} and a 16:8 light:dark cycle in a temperature-controlled growth room at 15 °C. The cultures were subsequently lost, both in Copenhagen and in Bremerhaven.

Light microscopy: Micrographs of live cells were taken with a Carl Zeiss Axio Imager.M2 microscope with a 63× oil immersion lens, using a Zeiss AxioCam digital camera (Zeiss, Oberkochen, Germany).

Epifluorescence: 1 ml cultured material was fixed with glutaraldehyde (1% final concentration), and filtered onto a black 0.2-μm polycarbonate filter. The filter was mounted on a glass slide with a small drop of VECTASHIELD® Mounting Medium with DAPI (Vector Laboratories, Burlingame, CA, US), and a coverslip on top. The mounted filter was kept dark at 4 °C overnight to allow the cell DNA to be stained well. Cells were studied in an inverted microscope (Olympus IX81, Japan) equipped with epifluorescence illumination and a disc-spinning unit for confocal imaging. This allowed observations of DAPI-stained DNA and chloroplast autofluorescence using the CellR software (Olympus, Japan). Micrographs were taken as z-stacks with a distance of 0.2 μm using a F-View II b/w digital camera (Olympus Soft Imaging System, Tokyo, Japan). Picture management was performed with the software Imaris 8.2 (Bitplane AG, Zürich, Switzerland).

Scanning electron microscopy (SEM): Taking culture densities of the strains into account, 3 and 1.5 ml of the two strains were fixed in 1% OsO_4 (final concentration) in distilled H_2O for 1 h. Cells were concentrated on an 8-μm mesh Costar nuclepore polycarbonate filter (Costar, Cambridge, MA, USA) in a Swinnex filter holder (Millipore, Darmstadt, Germany) and rinsed in distilled water for 20 min. Subsequently cells were dehydrated in a graded ethanol series with 10 min in each change of 30%, 50%, 70%, 90% at 5 °C and 99.9% at room temperature, followed by two changes of 30 min in 100% ethanol containing molecular sieves. Cells were dried using a Baltec CPD 030 critical point drier (Balzers, Liechtenstein), and mounted on metal stubs. They were coated with palladium-gold in a Jeol JFC-2300HR sputter coater and examined in a Jeol

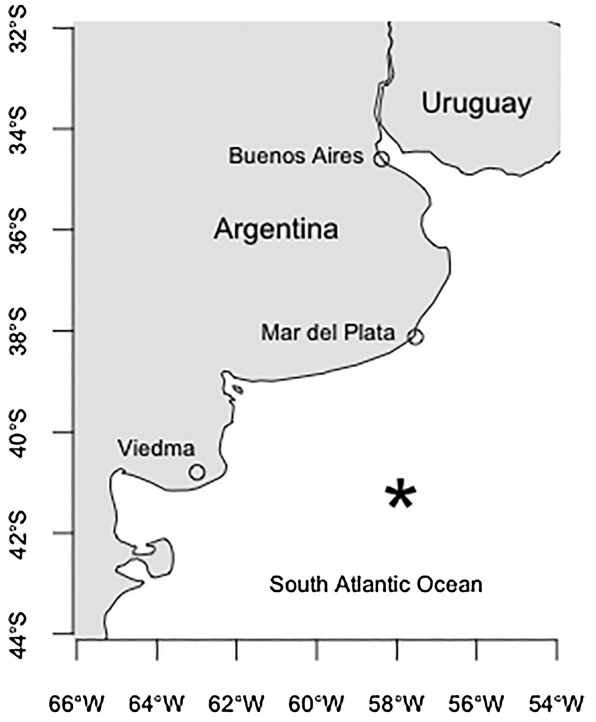

Figure 16. Map showing collection site of *Kirithra asteri* (*) off the coast of Argentina.

JSM-6333F field emission scanning electron microscope (Jeol Ltd, Tokyo, Japan).

Transmission electron microscopy (TEM): Cultured material from the two strains of *Kirithra asteri* was fixed for TEM by two different schedules.

Schedule 1: Cultured material was fixed in a mixture of 0.5% OsO_4 in filtered sterile seawater with a salinity of 30 and 2% glutaraldehyde (final concentrations) for 30 min. Cells were then concentrated by centrifugation for 5 min at 769 × *g* and the pellet was washed in L1 medium, three rinses of 10 min each. Post fixation was in 1% OsO_4 for 1.5 h, followed by a short rinse in distilled water. Material was subsequently dehydrated in a graded ethanol series (30%, 50%, 70% and 90%), 10 min in each concentration, followed by two 15-min changes in 100% ethanol containing molecular sieves. Dehydration was completed in two changes of propylene oxide for 5 min each and left overnight in a mixture of propylene oxide and Epon. The next morning a fresh amount of Epon was added and the following afternoon the pellet was transferred into an embedding mould with Epon and left to polymerize overnight in an oven at 60 °C.

Schedule 2: Cultured material was fixed in 2% glutaraldehyde in 0.1 M cacodylate buffer and 0.25 M sucrose (final concentrations) for 1 h. Material was spun down for 5 min at 2000 rpm (≈769 × *g*) and rinsed three times in cacodylate buffer with decreasing concentrations of sucrose. Post fixation was in 1% OsO_4 in cacodylate buffer for 1.5 h, followed by a short rinse in cacodylate buffer. The following steps were identical to schedule 1.

Overall, fixation schedule 1 preserved the cells best, both in regards to amphiesma and internal cell structures. Only cells in schedule 2 contained grana-like structures.

DNA extraction and PCR amplification: Thirteen ml of cultured cells was centrifuged at 2500 rpm for 10 min at 15 °C. The pellet was transferred to an Eppendorf tube and frozen at −18 °C until DNA extraction. The PowerPlant® Pro DNA Isolation Kit was used to obtain total genomic DNA following the manufacturer's recommendations (MO BIO Laboratories Inc., Carlsbad, CA, USA). To amplify ca 1480 base pairs of the nuclear-encoded large subunit (LSU) rDNA the forward primer D1R-F (Scholin et al. 1994) and the reverse primer 28-1483R (Daugbjerg et al. 2000) were used. The amplification kit was 5X Hot FIREPol Blend Master Mix from Solis BioDyne. PCR conditions were one initial cycle of denaturation at 95 °C for 12 min followed by 35 cycles each consisting of denaturation at 95 °C for 20 s, annealing at 54 °C for 40 s and extension at 72 °C for 40 s. The final step included extension at 72 °C for 5 min. To confirm the expected length of the PCR products we used electrophoresis with 1.5% agarose-casted gels run for 12 min at 150 V. PCR fragments were loaded into the gel stained by GelRed. PCR products were visualized using a gel documentation XR System from BioRad (Hercules, CA, USA) and compared to a 100-base-pair RAIN-BOW eXtended DNA ladder (BIORON GmbH, Ludwigshafen, Germany). To purify the amplified PCR products, we used ultrafiltration by applying the Nucleofast 96 PCR kit from Macherey-Nagel (GmbH & Co. KG, Düren, Germany), following the manufacturer's recommendations. The LSU rDNA sequence was determined in both directions using the amplification primers (D1R-F and 28-1483R) in addition to D3A, D3B (Nunn et al. 1996) and D2R (Scholin et al. 1994). The service provided by Macrogen (Amsterdam, Netherlands) was used for sequencing of the LSU rDNA gene.

Phylogeny: The nuclear-encoded LSU rDNA sequence of *Kirithra asteri* was supplemented to an alignment consisting of 102 other dinoflagellate species representing 68 genera. Jalview (ver. 14) (Waterhouse et al. 2009) was used to align (ClustalW) and further editing of the data matrix. The phylogenetic analyses were based on 1481 base pairs (including introduced gaps) and included Bayesian (BA) and maximum likelihood (ML). For BA, MrBayes (ver. 3.2.5 X64, Ronquist and Huelsenbeck 2003) was used with 5 million generations and sampling of trees for every 1,000 generations. Evaluation of the burn-in value was performed by plotting LnL scores as a function of generations. A burn-in was reached after 501,000 generations (conservative estimate) and this left 4,500 trees for construction of a 50% majority-rule consensus tree. jModelTest (ver. 2.1.3, Darriba et al. 2012) was used to obtain the parameter settings for ML analysis and the GTR-I-G was chosen as the best fit model for this data matrix among 88 different models examined. ML analyses used PhyML available at the Montpellier bioinformatics platform (http://www.atgc-montpellier.fr/phyml) and the robustness of the tree topology was evaluated with 500 bootstrap replications.

Acknowledgements

We thank Lis M. Frederiksen for assistance with TEM sectioning and Rut Akselman for sharing literature and for additional information on *Gymnodinium bonaerense*. We thank Mitsunori Iwataki for sharing unpublished images of *Gymnodinium* sp.2. ND thanks the Carlsberg Foundation and the VILLUM KANN RASMUSSEN for equipment grants.

Field sampling of UT was supported by the bilateral project MINCYT-DAAD (Ministerio de Ciencia, Tecnología e Innovación Productiva, Argentina, and Deutscher Akademischer Austauschdienst, Germany), code DA/13/04, Grant 57130105.

References

Abboud-Abi Saab M (1989) Les dinoflagellés des eaux côtières libanaises — espèces rares ou nouvelles du phytoplancton marin. Leban Sci Bull **5**:5–16

Akselman R (1985) Contribución al estudio de la familia Gymnodiniaceae Lemmermann (Dinophyta) del Atlántico Sudoccidental. Physis Secc A **43**:39–50

Bergholtz T, Daugbjerg N, Moestrup Ø, Fernaíndez-Tejedor M (2005) On the identity of *Karlodinium veneficum* and description of *Karlodinium armiger* sp. nov. (Dinophyceae), based on light and electron microscopy, nuclear-encoded LSU rDNA, and pigment composition. J Phycol **42**:170–193

Biecheler B (1952) Recherches sur les Peíridiniens. Bull Biol Fr Belg suppl **36**:1–149

Boutrup PV, Moestrup Ø, Tillmann U, Daugbjerg N (2016) *Katodinium glaucum* (Dinophyceae) revisited: proposal of new genus, family and order based on ultrastructure and phylogeny. Phycologia **55**:147–164

Bricheux G, Mahoney DG, Gibbs SP (1992) Development of the pellicle and thecal plates following ecdysis in the dinoflagellate *Glenodinium foliaceum*. Protoplasma **168**:159–171

Calado AJ, Moestrup Ø (2002) Ultrastructural study of the type species of *Peridiniopsis*, *Peridiniopsis borgei* (Dinophyceae), with special reference to the peduncle and flagellar apparatus. Phycologia **41**:567–584

Craveiro SC, Calado AJ, Daugbjerg N, Moestrup Ø (2009) Ultrastructure and LSU rDNA-based revision of *Peridinium* group palatinum (Dinophyceae) with the description of *Palatinus* gen. nov. J Phycol **45**:1175–1194

Craveiro SC, Moestrup Ø, Daugbjerg N, Calado AJ (2010) Ultrastructure and large subunit rDNA-based phylogeny of *Sphaerodinium cracoviense*, an unusual freshwater dinoflagellate with a novel type of eyespot. J Eukaryot Microbiol **57**:568–585

Craveiro SC, Pandeirada MS, Daugbjerg N, Moestrup Ø, Calado AJ (2013) Ultrastructure and phylogeny of *Theleodinium calcisporum* gen. et sp. nov., a freshwater dinoflagellate that produces calcareous cysts. Phycologia **52**:488–507

Darriba D, Taboada GL, Doallo R, Posada D (2012) jModelTest 2: More models, new heuristics and parallel computing. Nat Methods **9**:772

Daugbjerg N, Hansen G, Larsen J, Moestrup Ø (2000) Phylogeny of some of the major genera of dinoflagellates based on ultrastructure and partial LSU rDNA sequence data, including the erection of three new genera of unarmoured dinoflagellates. Phycologia **39**:302–317

de Salas MF, Laza-Martiínez A, Hallegraeff GM (2008) Novel unarmored dinoflagellates from the toxigenic family Kareniaceae (Gymnodiniales): Five new species of *Karlodinium* and one new *Takayama* from the Australian sector of the Southern Ocean. J Phycol **44**:241–257

de Salas MF, Bolch CJS, Botes L, Nash G, Wright SW, Hallegraeff GM (2003) *Takayama* gen. nov. (Gymnodiniales, Dinophyceae), a new genus of unarmored dinoflagellates with sigmoid apical grooves, including the description of two new species. J Phycol **39**:1233–1246

Dodge JD (1967) Fine structure of the dinoflagellate, *Aureodinium pigmentosum* gen. et. sp. nov. Brit Phycol Bull **3**:327–336

Dodge JD (1968) The fine structure of chloroplasts and pyrenoids in some marine dinoflagellates. J Cell Sci **3**:41–48

Dodge JD (1972) The ultrastructure of the dinoflagellate pusule: A unique osmo-regulatory organelle. Protoplasma **75**:285–302

Dodge JD (1975) A survey of chloroplast ultrastructure in the Dinophyceae. Phycologia **14**:253–263

Dodge JD, Crawford RM (1968) Fine structure of the dinoflagellate *Amphidinium carteri* Hulbert [sic]. Protistologica **4**:231–242

Dodge JD, Crawford RM (1971) A fine-structural survey of dinoflagellate pyrenoids and food-reserves. Bot J Linn Soc **64**:105–115

von Dürr G (1979) Elektronenmikroskopische Untersuchungen am Panzer von Dinoflagellaten. II. *Peridinium cinctum*. Arch Protistenkd **122**:88–120

Elbrächter M (1979) On the taxonomy of unarmoured dinophytes (Dinophyta) from the Northwest African upwelling region. "METEOR" Forsch.-Ergebnisse Reihe D, No **30**:1–22

Gao X, Dodge JD (1991) The taxonomy and ultrastructure of a marine dinoflagellate, *Scrippsiella minima* sp. nov. Brit Phycol J **26**:21–31

Gaudsmith JT, Dawes CJ (1972) The ultrastructure of several dinoflagellates with emphasis on *Gonyaulax polyedra* Stein and *Gonyaulax monilata* Davis. Phycologia **11**:123–132

Goímez F, Loípez-Garciía P, Takayama H, Moreira D (2015) *Balechina* and the new genus *Cucumeridinium* gen. nov. (Dinophyceae), unarmored dinoflagellates with thick cell coverings. J Phycol **51**:1088–1105

Gómez F, Nagahama Y, Fukuyo Y, Furuya K (2004) Observations on *Ceratoperidinium* (Dinophyceae). Phycologia **43**:416–421

Gu H, Luo Z, Zhang X, Xu B, Fang Q (2013) Morphology, ultrastructure and phylogeny of *Takayama xiamenensis* sp. nov. (Gymnodiniales, Dinophyceae) from the East China Sea. Phycologia **52**:256–265

Gu H, Luo Z, Mertens KN, Price AM, Turner RE, Rabalais NN (2015) Cyst-motile stage relationship, morphology, ultrastructure, and molecular phylogeny of the gymnodinioid dinoflagellate *Barrufeta resplendens* comb. nov., formerly known as *Gyrodinium resplendens*, isolated from the Gulf of Mexico. J Phycol **51**:990–999

Guillard RRL, Hargraves PE (1993) *Stichochrysis immobilis* is a diatom, not a chrysophyte. Phycologia **32**:234–236

Hansen G, Daugbjerg N (2004) Ultrastructure of *Gyrodinium spirale*, the type species of *Gyrodinium* (Dinophyceae), including a phylogeny of *G. dominans*, *G. rubrum* and *G. spirale* deduced from partial LSU rDNA sequences. Protist **155**:271–294

Hansen G, Daugbjerg N (2011) *Moestrupia oblonga* gen. & comb. nov. (Syn.: *Gyrodinium oblongum*), a new marine dinoflagellate genus characterized by light and electron microscopy, photosynthetic pigments and LSU rDNA sequence. Phycologia **50**:583–599

Hansen G, Moestrup Ø (2005) Flagellar apparatus and nuclear chambers of the green dinoflagellate *Gymnodinium chlorophorum*. Phycol Res **53**:169–181

Hansen G, Daugbjerg N, Franco JM (2003) Morphology, toxin composition and LSU rDNA phylogeny of *Alexandrium minutum* (Dinophyceae) from Denmark, with some morphological observations on other European strains. Harmful Algae **2**:317–335

Hansen G, Moestrup Ø, Roberts KR (1996) Fine-structural observations on *Gonyaulax spinifera* (Dinophyceae), with special emphasis on the flagellar apparatus. Phycologia **35**:354–366

Hansen G, Moestrup Ø, Roberts KR (2000) Light and electron microscopical observations on the type species of *Gymnodinium*, *G. fuscum* (Dinophyceae). Phycologia **39**:365–376

Höhfeld I, Melkonian M (1992) Amphiesmal ultrastructure of dinoflagellates: a reevaluation of pellicle formation. J Phycol **28**:82–89

Hoppenrath M, Murray S, Sparmann SF, Leander BS (2012) Morphology and molecular phylogeny of *Ankistrodinium* gen. nov. (Dinophyceae), a new genus of marine sand-dwelling dinoflagellates formerly classified within *Amphidinium*. J Phycol **48**:1143–1152

Horiguchi T, Sukigara C (2005) *Pyramidodinium atrofuscum* gen. et sp. nov. (Dinophyceae), a new marine sand-dwelling coccoid dinoflagellate from tropical waters. Phycol Res **53**:247–254

Horiguchi T, Tamura M, Katsumata K, Yamaguchi A (2012) *Testudodinium* gen. nov. (Dinophyceae), a new genus of sand-dwelling dinoflagellates formerly classified in the genus *Amphidinium*. Phycol Res **60**:137–149

Iwataki M, Hansen G, Moestrup Ø, Matsuoka K (2010) Ultrastructure of the harmful unarmored dinoflagellate *Cochlodinium polykrikoides* (Dinophyceae) with reference to the apical groove and flagellar apparatus. J Eukaryot Microbiol **57**: 308–321

Jang SH, Jeong HJ, Moestrup Ø, Kang NS, Lee SY, Lee KH, Seong KA (2017) *Yihiella yeosuensis* gen. et sp. nov. (Suessiaceae, Dinophyceae), a novel dinoflagellate isolated from the coastal waters of Korea. J Phycol **53**:131–145

Jeong HJ, Jang SH, Moestrup Ø, Kang NS, Lee SY, Potvin E, Noh JH (2014) *Ansanella granifera* gen. et sp. nov. (Dinophyceae), a new dinoflagellate from the coastal waters of Korea. Algae **29**:75–99

Kang NS, Jeong HJ, Moestrup Ø, Park TG (2011) *Gyrodiniellum shiwhaense* n. gen., n. sp., a new planktonic heterotrophic dinoflagellate from the coastal waters of Western Korea: morphology and ribosomal DNA gene sequence. J Eukaryot Microbiol **58**:284–309

Kang NS, Jeong HJ, Moestrup Ø, Shin W, Nam SW, Park JY, de Salas MF, Kim KW, Noh JH (2010) Description of a new planktonic mixotrophic dinoflagellate *Paragymnodinium shiwhaense* n. gen., n. sp. from the coastal waters off Western Korea: morphology, pigments, and ribosomal DNA gene sequence. J Eukaryot Microbiol **57**:121–144

Kite GC, Dodge JD (1988) Cell and chloroplast ultrastructure in *Gyrodinium aureolum* and *Gymnodinium galatheanum*. Two marine dinoflagellates containing an unusual carotenoid. Sarsia **73**:131–138

Kofoid CA (1931) Report of the biological survey of Mutsu Bay. 18. Protozoan Fauna of Mutsu Bay. Subclass Dinoflagellata; Tribe Gymnodinoidae. Scientific Reports of Tohoku University, Series Ser 4 **6**: 1–43

Kofoid CA, Swezy O (1921) The Free-Living Unarmored Dinoflagellata. Memoirs of the University of California **5**:1–564

Konovalova GV (2003) The life history of *Gyrodinium falcatum* and validity of *Pseliodinium vaubanii* (Dinophyceae). Russ J Mar Biol **29**:167–170

Larsen J (1988) An ultrastructural study of *Amphidinium poecilochroum* (Dinophyceae), a phagotrophic dinoflagellate feeding on small species of cryptophytes. Phycologia **27**:366–377

Loeblich AR III (1980) Dinoflagellate Nomenclature. Taxon **29**:321–328

Lom J, Schubert G (1983) Ultrastructural study of *Piscinoodinium pillulare* (Schäperclaus, 1954) Lom, 1981 with special emphasis on its attachment to the fish host. J Fish Dis **6**:411–428

Maranda L, Shimizu Y (1996) *Amphidinium operculatum* var. nov. *gibbosum* (Dinophyceae). A free-swimming marine species producing cytotoxic metabolites. J Phycol **32**:873–879

Margalef R (1969) Composicioín especiífica del fitoplancton de la costa catalano-levantina (Mediterraíneo occidental) en 1962-1967. Investigacion Pesquera **33**:345–380

Maruyama T (1982) Fine structure of the longitudinal flagellum in *Ceratium tripos*, a marine dinoflagellate. J Cell Sci **58**:109–123

Melkonian M, Höhfeld I (1988) Amphiesmal ultrastructure in *Noctiluca miliaris* Suriray (Dinophyceae). Helgoländer Meeresunters **42**:601–612

Moestrup Ø (1982) Flagellar structure in algae: a review, with new observations particularly on the Chrysophyceae, Phaeophyceae (Fucophyceae), Euglenophyceae, and *Reckertia*. Phycologia **21**:427–528

Moestrup Ø, Daugbjerg N (2007) On Dinoflagellate Phylogeny and Classification. In Brodie J, Lewis J (eds) Unravelling the Algae: The Past, Present and Future of Algal Systematics. Systematics Association Special Volumes **vol. 75**. CRC Press, Taylor & Francis Group, London, pp 215–230

Moestrup Ø, Lindberg K, Daugbjerg N (2009) Studies on woloszynskioid dinoflagellates V. Ultrastructure of *Biecheleriopsis* gen. nov., with description of *Biecheleriopsis adriatica* sp. nov. Phycol Res **57**:221–237

Moestrup Ø, Hakanen P, Hansen G, Daugbjerg N, Ellegaard M (2014) On *Levanderina fissa* gen. & comb. nov. (Dinophyceae) (Syn. *Gymnodinium fissum*, *Gyrodinium instriatum*,

Gyr. uncatenum), a dinoflagellate with a very unusual sulcus. Phycologia **53**:265–292

Morrill LC (1984) Ecdysis and the location of the plasma membrane in the dinoflagellate *Heterocapsa niei*. Protoplasma **119**:8–20

Morrill LC, Loeblich AR III (1981) The dinoflagellate pellicular wall layer and its occurrence in the division Pyrrhophyta. J Phycol **17**:315–323

Morrill LC, Loeblich AR III (1983) Ultrastructure of the dinoflagellate amphiesma. Int Rev Cytol **82**:151–180

Nunn GB, Theisen BF, Christensen B, Arctander P (1996) Simplicity-correlated size growth of the nuclear 28S ribosomal RNA D3 expansion segment in the crustacean order Isopoda. J Mol Evol **42**:211–223

Omura T, Iwataki M, Borja VM, Takayama H, Fukuyo Y (2012) Marine Phytoplankton of the Western Pacific. Kouseisha Kouseikaku Co., Ltd., Tokyo, 160 p

Reñé A, de Salas MF, Camp J, Balagué V, Garcés E (2013) A new clade, based on partial LSU rDNA sequences, of unarmoured dinoflagellates. Protist **164**:673–685

Roberts KR, Roberts JE (1991) The flagellar apparatus and cytoskeleton of dinoflagellates, a comparative overview. Protoplasma **164**:105–122

Roberts KR, Hansen G, Taylor JFR (1995) General ultrastructure and flagellar apparatus architecture of *Woloszynskia limnetica* (Dinophyceae). J Phycol **31**:948–957

Ronquist F, Huelsenbeck JP (2003) MrBayes 3: Bayesian phylogenetic inference under mixed models. Bioinformatics **19**:1572–1574

Sampedro N, Fraga S, Penna A, Casabianca S, Zapata M, Grünewald CF, Rioboí P, Camp J (2011) *Barrufeta bravensis* gen. nov. sp. nov. (Dinophyceae): A new bloom-forming species from the Northwest Mediterranean Sea. J Phycol **47**:375–392

Schnepf E, Elbrächter M (1999) Dinophyte chloroplasts and phylogeny — a review. Grana **38**:81–97

Scholin C, Herzog M, Sogin M, Anderson DM (1994) Identification of group and strain specific genetic markers for globally distributed *Alexandrium* (Dinophyceae). II. Sequence analysis of a fragment of the LSU rRNA gene. J Phycol **30**: 999–1011

Schütt F (1895) Die Peridineen der Plankton-Expedition. Ergebnisse der Plankton-Expedition der Humboldt-Stiftung **4**:1–170

Sournia A (1972). Une période de poussées phytoplanctoniques près de Nosy-Bé (Madagascar) en 1971. Espèces rares ou nouvelles du phytoplancton. Cahiers de l'Office de la Recherche Scientifique et Technique Outre-Mer. Paris. Série Océanographique **10**:151–159

Sparmann SF, Leander BS, Hoppenrath M (2008) Comparative morphology and molecular phylogeny of *Apicoporus* n. gen.: a new genus of marine benthic dinoflagellates formerly classified within *Amphidinium*. Protist **159**:383–399

Takahashi K, Moestrup Ø, Jordan RW, Iwataki M (2015) Two new freshwater woloszynskioids *Asulcocephalium miricentonis* gen. et sp. nov. and *Leiocephalium pseudosanguineum* gen. et sp. nov. (Suessiaceae, Dinophyceae) lacking an apical furrow apparatus. Protist **166**:638–658

Takano Y, Yamaguchi H, Inouye I, Moestrup Ø, Horiguchi T (2014) Phylogeny of five species of *Nusuttodinium* gen. nov. (Dinophyceae), a genus of unarmoured kleptoplastidic dinoflagellates. Protist **165**:759–778

Tamura M, Horiguchi T (2005) *Pileidinium ciceropse* gen. et sp. nov. (Dinophyceae), a sand-dwelling dinoflagellate from Palau. Eur J Phycol **40**:281–291

Tillmann U, Elbrächter M, John U, Krock B, Cembella A (2010) *Azadinium obesum* (Dinophyceae), a new nontoxic species in the genus that can produce azaspiracid toxins. Phycologia **49**:169–182

Waterhouse AM, Procter JB, Martin DMA, Clamp M, Barton GJ (2009) Jalview Version 2 — a multiple sequence alignment editor and analysis workbench. Bioinformatics **25**:1189–1191

Wilcox LW, Wedemayer GJ, Graham LE (1982) *Amphidinium cryophilum* sp. nov. (Dinophyceae) a new freshwater dinoflagellate. II. Ultrastructure. J Phycol **18**:18–30

Yamada N, Terada R, Tanaka A, Horiguchi T (2013) *Bispinodinium angelaceum* gen. et sp. nov. (Dinophyceae), a new sand-dwelling dinoflagellate from the seafloor off Mageshima Island, Japan. J Phycol **49**:555–569

Yuasa T, Horiguchi T, Mayama S, Takahashi O (2016) *Gymnoxanthella radiolariae* gen. et sp. nov. (Dinophyceae), a dinoflagellate symbiont from solitary polycystine radiolarians. J Phycol **52**:89–104